A specific role for Importin-5 and NASP in the import and nuclear hand-off of monomeric H3

Alonso J. Pardal and Andrew J. Bowman[1,✉]

[1]Division of Biomedical Sciences, Warwick Medical School, University of Warwick, Gibbet Hill Road, Coventry, CV4 7AL, UK

Core histones package chromosomal DNA and regulate genomic transactions, with their nuclear import and deposition involving importin-β proteins and a dedicated repertoire of histone chaperones. Previously, a histone H3-H4 dimer has been isolated bound to Importin-4 (Imp4) and and the chaperone ASF1, suggesting H3 and H4 fold together in the cytoplasm before nuclear import. However, other studies have shown the existence of monomeric H3 in the nucleus, indicating a post import folding pathway. Here we report that the predominant importin associated with cytoplasmic H3 is Importin-5 (Imp5), which hands-off its monomeric cargo to nuclear sNASP. Imp5, in contrast to Imp4, binds to both H3 and H4 containing constitutively monomeric mutations and binds to newly synthesised, monomeric H3 tethered in the cytoplasm. Constitutively monomeric H3 retains its interaction with NASP, whereas monomeric H4 retains interactions specifically with HAT1 and RBBP7. High-resolution separation of NASP interactors shows the 's' isoform but not the 't' isoform associates with monomeric H3, whilst both isoforms associate with H3-H4 dimers in at least three discrete multi-chaperoning complexes. *In vitro* binding experiments show mutual exclusivity between sNASP and Imp5 in binding H3, suggesting direct competition for interaction sites, with the GTP-bound form of Ran required for histone transfer. Finally, using pulse-chase analysis we show that cytoplasm-tethered histones do not interact with endogenous NASP until they reach the nucleus, whereupon they bind rapidly. We propose an Imp5-specific import pathway for monomeric H3 that hands off to sNASP in the nucleus, with a parallel H4 pathway involving Imp5 and the HAT1-RBBP7 complex, followed by nuclear folding and hand-off to deposition factors.

Histone H3, H4 | histone chaperone | importins | proteomics | chromatin
Correspondence: ***a.bowman.1@warwick.ac.uk***

Introduction

Histones are one of the most abundance class of proteins within the cell, with nuclear import and deposition into chromatin being a major challenge during S-phase (1, 2). Import, folding, and delivery of histones to sites of incorporation in a timely manner can thus impact a broad range of genomic processes and are of great current interest (1, 3–6).

Histones are synthesised in the cytoplasm and translocate to the nucleus associated with importin proteins (also known as karyopherins) (7). Once in the nucleus, importins interact with RanGTP leading to the unloading of their cargo (8). Work on different organisms has cemented the notion that, despite certain redundancy, most importin-histone interactions are specific (9–13). For instance, H2A and H2B have been shown to associate with Importin-9 (Imp9) (11, 14), whereas, H3 and H4 have been shown to associate with Imp4 (15–17) and, to a lesser extent, Imp5 (17). Similar selectivity occurs in yeast, with H3 and H4 shown to interact with homologs Kap123 and Kap121, respectively (12). Interestingly, *in vitro* H3-H4 have broader binding profiles (18), and can be imported by a number of importins in reconstituted systems using isolated nuclei (10).

Histone chaperones also associate promptly with newly synthesised histones, providing an environment for solubility and ensuring correct folding before targeting towards sites of DNA deposition (1, 2, 6). Numerous factors have been isolated in complex with H3 and H4 from cytosolic extracts (15, 16, 19, 20); however, as many of these factors are overwhelmingly found in the nucleus under native conditions, it is not clear how well cytosolic extracts represent the true cytoplasm of the cell (21–23).

Nuclear Autoantigenic Sperm Protein was first identified as an H1-binding protein expressed in testis (tNASP) (24) that also interacted with HSP90 (25). In dividing somatic cells a shorter splice isoform is prevalent (sNASP) (26), whereas both isoforms often occur in transformed cell lines (16). Subsequently, NASP has been shown to interact predominantly with H3 and H4 (15, 16, 19, 27). NASP displays multivalent interactions with its histone cargo, binding to a peptide epitope at the C-terminus of H3 via a canonical TPR-peptide interaction (28, 29), and to an N-terminal region of H3 via a site on the surface of the TPR domain (27, 29, 30). The latter interaction is structurally compatible with H3-H4 dimer binding in conjunction with ASF1. However, the TPR-H3 C-terminal peptide interaction is structurally exclusive (29–31). These structural analyses may partly explain why NASP binds a supra-stoichiometric amount of H3 over H4; that is NASP binds to both an H3 monomeric and an H3-H4 dimeric pool of histones (21).

Despite significant investigation, it is still not clear where, and in association with what factors, folding of newly synthesised H3-H4 occurs in the cell (2). Isolation of an H3-H4 dimer bound to Imp4 and ASF1 in cytosolic extracts has been accepted as evidence for H3 and H4 folding in the cytoplasm (15–17). However, it has been shown that such extracts often contain soluble nucleoplasmic components, due to the difficulty in rupturing the plasma membrane whilst leaving the nuclear membrane intact (21–23) , and thus how these extracts relate to the cytoplasm is not clear. H3 and H4 tethered in the cytoplasm immediately after translation remain monomeric and do not fold with their endogenous counterpart (21), whilst supra-stoichiometric binding of H3 by NASP suggests the presence of a stable monomeric pool

DRAFT

of H3 (21). Furthermore, monomeric histones serve as effective substrates for nuclear import in isolated nuclei (10), suggesting a monomeric substrate can be recognised by importins, at least in permeabilised cells.

In this study we investigate the interactome of histones H3 & H4 using constitutive monomeric mutants and post-synthesis trapping using the RAPID-release approach. We identify Imp5 as a primary binder of monomeric H3 and H4 in the cytoplasm, with histone-specific interactions maintained by a number of histone chaperones. Fractionation of fractionate NASP-associated complexes, revealed a stable NASP-H3 monomer population, roughly equal in size to that of NASP-H3-H4 containing complexes. NASP and Imp5 binding are mutually exclusive, with *in vitro* experiments showing RanGTP is necessary for hand-off to occur. Lastly, we show that NASP associates with H3 rapidly after its import, suggesting it is a receptor for monomeric H3 after transfer from Imp5. These findings support a model in which newly synthesised H3 and H4 are imported as monomers bound to Imp5 and fold in the nucleus once associated with their histone chaperones.

Results

Constitutively monomeric H3 & H4 translocate to the nucleus and retain bind to a subset of histone chaperones & importins.

To probe factors that interact with monomeric histones, we designed mutations that preclude folding of the heterodimer, trapping histones in their otherwise transient, post-synthesis state. As any mutation may omit potential binders, two divergent strategies were taken: 1 - breaking the $\alpha 2$ helix of the histone fold domain by insertion of three glycine residues (helix-breaker mutations, HB), and 2 - disruption of the histone fold by substituting three hydrophobic core residues (fold-disruptor mutations, FD), (Fig. 1A and B).

To test their cellular localisation, histone mutants were fused to eGFP and transiently expressed in HEK293-F cells (Fig. 1C). Both sets of mutants showed nuclear fluorescence in interphase cells, demonstrating they are import-competent, but did not colocalise to mitotic chromosomes, suggesting they are not incorporated into chromatin (Fig. 1C). We further tested chromatin incorporation using Fluorescence Recovery After Photo-bleaching (FRAP) analysis (Fig. 1D). Chromatinised histones should turnover very slowly, whilst soluble histones should recover almost immediately. Indeed, we found while recovery of WT histones in the bleached region was slow, recovery of mutant histones occurred within seconds. We therefore conclude that non-dimerising mutants of H3 and H4 are imported into the nucleus, but are not incorporated into chromatin.

To test if the mutants can fold with their endogenous counterpart, we purified C-terminal eGFP fusions using single step, GFP-Trap® pulldowns (Fig. 1E). As endogenous histones are unusually small, they are well-resolved from other interacting proteins and can be unambiguously identified by coomassie staining after SDS-PAGE. Whilst WT H3.1-eGFP pulled down H4, and H4-eGFP pulled down H3, mutant histones failed to pull down any of their endogenous counterparts (Fig. 1E).

To further investigate the associations of mutant histones we performed western blots, probing the pulldowns with antibodies for a number of known interacting factors (Fig. 1F). Whilst WT H3 interacted with the full cohort of probed histone chaperones, H3 mutants only interacted with NASP (both s and t isoforms) and Imp5, but surprisingly not Imp4 (Fig. 1F). H4 similarly lost the majority of its interacting proteins, retaining only the HAT1 complex (HAT1 & RBBP7) and Imp5, but not Imp4 (Fig. 1F). Taken together, these findings show that constitutively monomeric mutants are imported into the nucleus, show differences in their chaperone profiles, but share the common binding of Imp5 over Imp4.

Interactomes of histone monomer mutants.

To unbiasedly identify factors interacting with monomeric H3 and H4 we performed affinity purification followed by mass spectrometry (Fig. 2A-D). Plotting normalised total precursor intensity of WT against mutant, we confirmed Imp5 and NASP retains interaction with monomeric H3, and Imp5 and HAT1-RBBP7 retains interaction with monomeric H4 (Fig. 2A-D). Notably, binding profiles are similar across both types of mutant (HD or FB) and reproducible across three biological replicates (Fig. 2E and F).

In addition, we identified a number of HSP70 family members associating with both monomeric & WT H3 (HSPA1B, HSPA6, HSPA8) and H4 (HSPA1B, HSPA8), confirming previously identified interactions (15) and highlighting the cross-talk between heat shock chaperones and the histone chaperoning network (32). The HSP70-interacting protein DNAJC9 showed a strong preference for WT histones in both H3 and H4 pulldowns, as would be expected from its recently solved structure with an H3-H4 dimer (32). Similarly, factors involved in the direct deposition of histones onto DNA (CAF1 complex, DAXX, ASF1A-B, MCM2) demonstrated strong preference for WT histones, again, as one might expect from their structural characterisation with H3-H4 dimers (33–38).

Intriguingly, two recently discovered histone chaperones UBR7 (39) and C1QBP (40) retained interactions with monomeric histones, with UBR7 showing specificity for histone H3 while C1QBP interacted with both H3 and H4. Furthermore, NAP1-like proteins NAP1L1 and NAP1L4 also bound to monomeric histones, albeit at much lower levels than other chaperones. Taken together, these results show that monomeric mutants of H3 and H4 retain distinct interaction profiles compared to WT, and confirms Imp5, but not Imp4, as interacting with histones in their monomeric state.

NASP forms discrete H3 monomer and H3-H4 dimer containing complexes.

NASP can chaperone a monomer of H3 *in vitro* (31), bind to an epitope obscured in the H3-H4 interface (28, 29), and pulldown supra-stoichiometric amounts of H3 over H4 when isolated from HeLa cell extracts (21). To probe the NASP-associated histone pool at endogenous levels, we tagged NASP at its endogenous locus with TEV-cleavable (TEVcs)

DRAFT

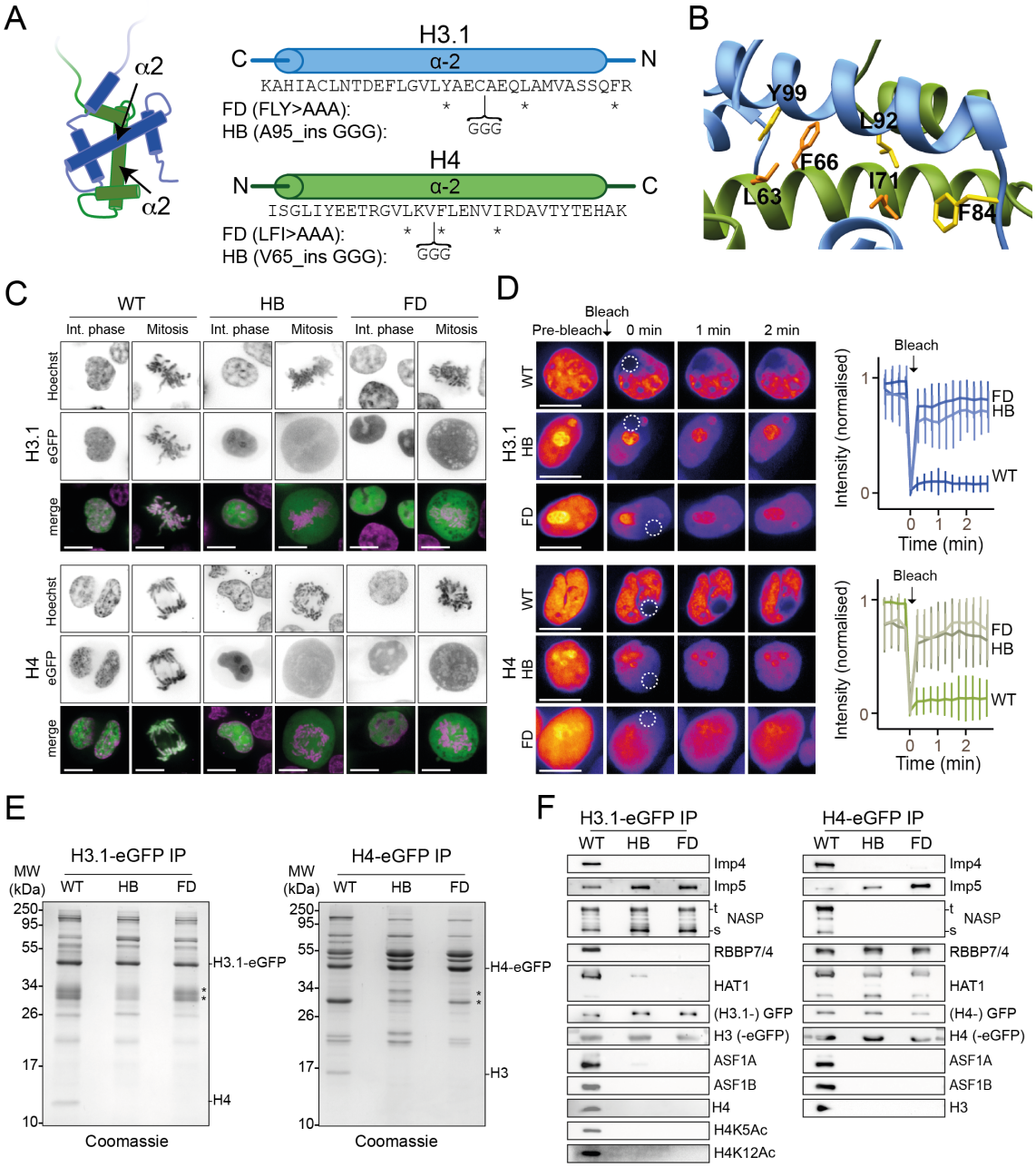

Fig. 1. H3 and H4 dimerisation mutants translocate to the nucleus but do not incorporate into chromatin. A: Positions of Fold-Disruptor (FD) substitutions (asterisks) and Helix-Breaker (HB) insertions (brackets). **B**: Positions of the fold-disruptor mutations superimposed on the H3-H4 heterodimer (PDB: 2HUE). Residues targeted are shown in yellow for H3 and in orange for H4. **C**: Non-folding mutants were expressed as eGFP C-terminal fusions and transiently transfected in HEK293-F cells. Mutants localise to the nucleus similar to WT, but do not incorporate into chromatin as visualised by cytoplasmic fluorescence during mitosis. Scale bar indicates 10 μm. **D**: FRAP analysis of wild-type and mutant histones. Bleached regions of the nuclei at t= 0 min are indicated. Immediate recovery of fluorescence after bleaching shows that the histone mutants are not chromatin-bound as are their wild-type counterparts. Note, histone mutants have a tendency to accumulate in nucleoli. **E**: Wild-type and mutant eGFP fusions were affinity-purified using an anti-GFP nanobody, separated by SD-PAGE and stained with Coomassie. Positions of tagged and endogenous histones are indicated. Asterisk indicate free GFP and partial degradation products. **F**: Western blot analysis of immunoprecipitated wild-type and histone mutants as shown in E probed for known histone interactors (HB, Helix Breaker mutation; FD, Fold Disruptor mutation).

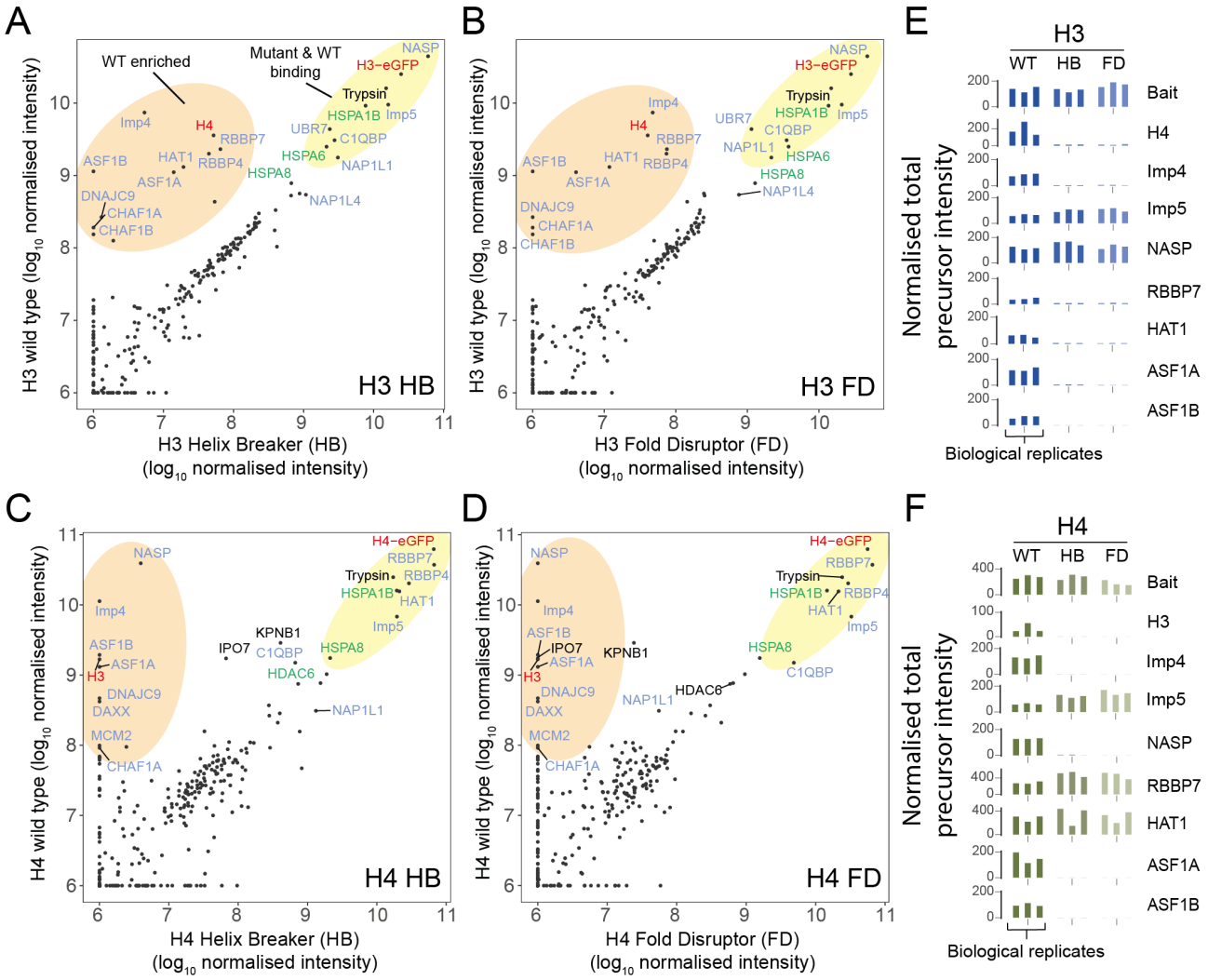

Fig. 2. Proteomic analysis of wild type and monomeric histone mutants A-D: Mutant versus WT scatter plots of normalised total precursor intensity from H3 vs. HB (A), H3 vs. FD (B), H4 vs. HB (C) and H4 vs. FB (D). Average of three experiments (log_{10}). By plotting mutants versus WT, factors that interact at similar levels will lie on the diagonal, with those that have preference for the dimer or monomer to fall above or below the diagonal, respectively. Circled regions show factors that are enriched for the wild-type (orange) or that are equally enriched on the wild type and mutant (yellow). Previously reported histone-binding proteins are coloured in blue, with Hsc70 family members coloured in green. Histones are coloured in red. **E-F**: Alternative representation of proteomics data showing quantitative values (normalised total precursor intensity) on a linear scale ($1x10^6$) for each biological replicate of key factors identified in A-D (HB, Helix Breaker mutation; FD, Fold Disruptor mutantion).

eGFP using CRISPR (Fig. 3A). For comparison of H3-H4 dimer binding, we also knocked in a SpotTag-mCherry-3Ccs tag in frame with the first exon of ASF1B (Fig. 3A, Fig. S2), and purified these constructs using a single step GFP-/RFP-Trap® pulldown, alongside sNASP expressed transiently in HEK293-F cells. sNASP over-expression in HEK293-F cells and NASP expression from its endogenous locus in HeLa showed at least a 2-fold molar excess of H3 over H4, whereas ASF1 showed close to equimolar amounts in each case (Fig. 3B & C), demonstrating that under endogenous conditions NASP binds to a suprachoichiometric amount of H3 over H4.

To determine if this excess of H3 relates to a sub-pool of NASP-H3 monomer, we performed biochemical fractionation of sNASP-containing complexes from HEK293-F cells (insufficient material prevented us using endogenously tagged HeLa lines, however, the similar ratios of H3 to H4 in both lines suggests transient expression in HEK293 is representative of the endogenous scenario). Associated complexes were affinity captured using GFP-Trap® resin before separation on either a glycerol gradient (Fig. 3D) or by native PAGE (Fig. 3E). SDS-PAGE analysis of gradient fractions revealed a sNASP-H3 monomer complex that could be unambiguously separated from other H3-H4 containing complexes (Fig. 3, fractions 6-8, arrows). Western blotting confirmed the presence of sNASP and H3 in this complex, and the absence of H4, in addition to the absence co-chaperones HAT1, RBBP7, ASF1A and ASF1B, all of which eluted with the H3-H4 dimer displaying the H4K5Ac mark of newly synthesised histones (Fig. 3D). Interestingly, UBR7 came down with sNASP, but did not migrate with the main sNASP-H3 species, as may be expect from our monomeric histone mutant analyses (Fig. 2A and B), but overlapped with the broad sNASP co-chaperone peak (Fig. 3D).

Native PAGE resulted in greater separation compared to glycerol gradient centrifugation, with individual bands represent-

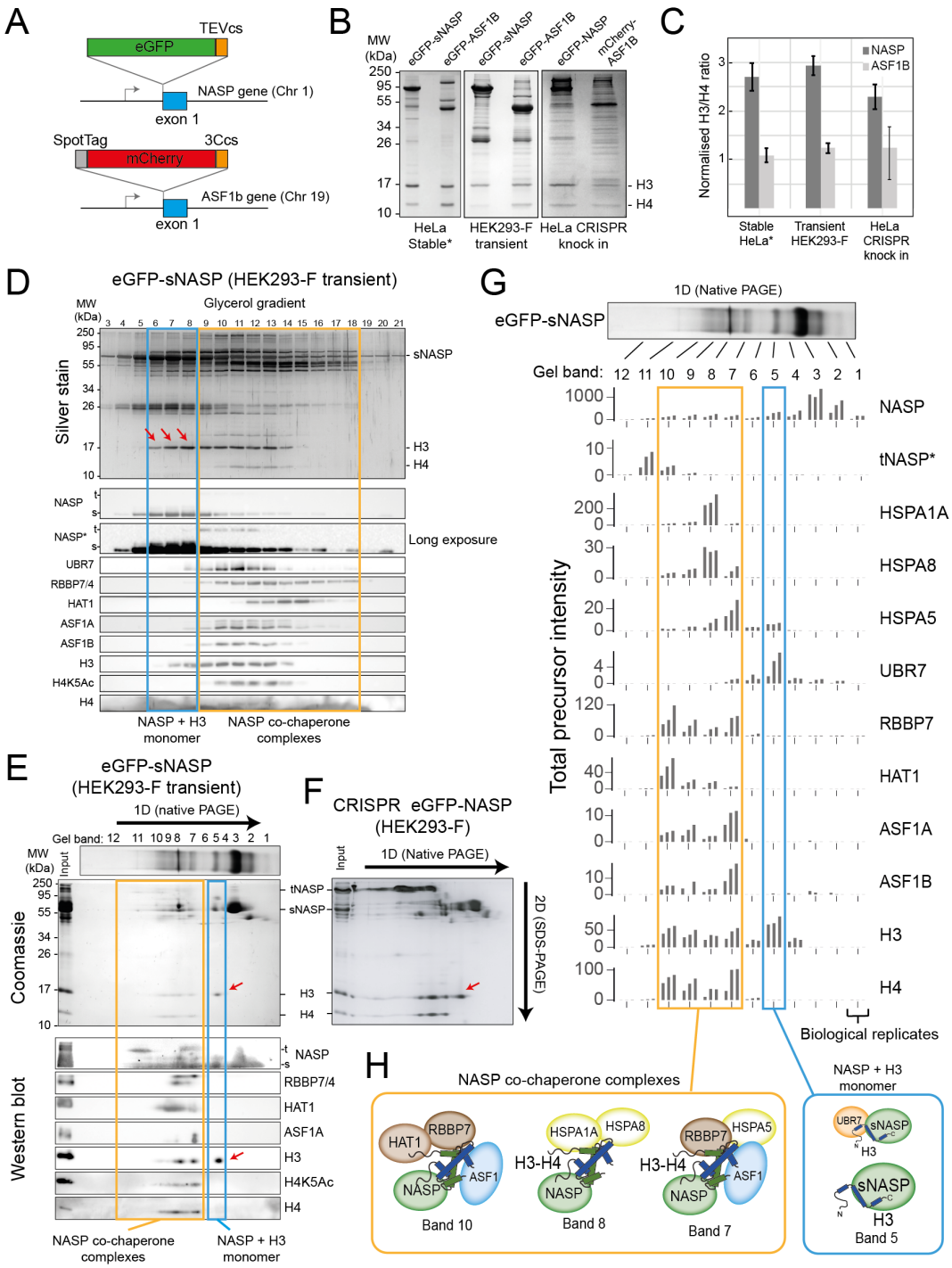

Fig. 3. NASP associates with an H3 monomer and H3-H4 dimers in discrete, multi-chaperone complexes. **A**: CRISPR knock-in tagging scheme. Endogeous NASP was tagged on exon 1 with eGFP-TEVcs and ASF1B with SpotTag-mCherry-3Ccs. **B**: Histone chaperone immunoprecipitations separated by 15% SDS–PAGE and stained with Coomassie, for eGFP-sNASP and eGFP-ASF1B as stable HeLa cell lines, HEK293-F transient expression and CRISPR knock-in (as described in A). Asterisks mark previously published data (21). **C**: Ratios of H3 compared to H4 associated with NASP and ASF1 from extracts stably expressed in a HeLa cell line, transiently expressed in HEK293-F cells or endogenously expressed in a CRISPR knock in HeLa cell line. Background-corrected densitometry profiles for H3 and H4 were compared with purified recombinant H3-H4 dimers (n = 3, error bars = s. d.). **D**: Fractionation by ultra-centrifugation on a glycerol gradient (4-20%) of immunoprecipitated eGFP-sNASP from transiently transfected HEK293-F cells (as in B) followed by SDS-PAGE, silver staining (top) and western blot (bottom). Lane numbers correspond to glycerol fractions. Note, a species containing H3 but not H4 is clearly discernible (red arrows). **E**: Native gel separation of immunoprecipitated eGFP-sNASP transiently expressed in HEK293-F cells (as in B) followed by SDS-PAGE, Coomassie staining (top) and western blot (bottom). Blots were probed for known NASP-interacting factors. Note, a species containing H3 but not H4 is clearly discernible (red arrows). Band numbers correspond to gel sections that were analysed by mass spectrometry (as shown in G). **F**: 2D native/SDS-PAGE as shown in E, but using eGFP-NASP pulldowns from a HEK293-F knock-in cell population created identically to that show in A. Note, the tNASP isofrom is more prevalent, but only the sNASP isoform co-migrates with monomeric H3. **G**: Mass spectrometry identification of sNASP-interacting factors from gel slices shown in E (Total precursor intensity). tNASP-specific peptides are shown separately to pan-NASP peptide. **H**: Diagrammatic representation of NASP-containing complexes.

ing distinct complexes being observed (Fig. 3E). To identify components of each band, further separation in a second dimension under denaturing conditions was performed before staining with Coomassie or probing by Western blot (Fig. 3E). Free sNASP is clearly visible as the major species in band 3, with partially degraded versions as minor species in band 1 and 2. sNASP-bound H3, without H4, migrated as a separate species in band 5 (arrow), whereas H3-H4 and co-chaperones eluted in various species from bands 6-11 (Fig. 3E).

Curiously, a minor, higher molecular weight band was detected in the anti-NASP western blot under a long exposure, which runs at a size indicative of the tNASP isoform (Fig. 3E). This was intriguing as only the shorter sNASP isoform was expressed as the eGFP-fusion and may relate to a low level of dimerisation with the endogeous protein, which has been suggested from the crystal structure (29, 30) and biochemical analysis (41). Interestingly, only the s, and not the t, isoform co-migrated with the H3 monomer band. To investigate this further we used a HEK293-F CRISPR knock-in cell line to separate complexes from both isoforms under endogenous expression levels (Fig. 3F). As expected the CRIPSR knock-in showed similar amounts of both splice isoforms, and again only the sNASP isoform co-migrated with an H3 monomer species (Fig. 3F, arrow), suggesting that monomer binding may be an sNASP-specific function.

To more accurately assign components to each species, bands from sNASP 1D native gels were excised and subjected to mass spectrometry (Fig. 3G). Label-free quantification (LFQ) of total precursor intensity for top hits (full list in Fig.S3 and Table S4) were plotted for each band in sequence, with the corresponding profiles revealing distinct sub-complexes associated with sNASP (Fig. 3G and H). Band 5 was validated as containing monomeric H3 bound to sNASP without H4 and, surprisingly, UBR7. The UBR7 containing complex was estimated as roughly one tenth of the NASP-H3 signal, which may explain the elution of UBR7 in the glycerol gradient: that is, the minor NASP-H3-UBR7 complex elutes separately from the major NASP-H3 complex on a glycerol gradient, but similarly in native PAGE. Band 7 contained peak signals for the HSC70 protein HSPA5, in addition to the histone chaperones RBBP7 and ASF1A-B and both H3 and H4, whereas band 8 contained peak signals for HSPA1A and HSPA8 together with a smaller proportion of H3 and H4. The NASP complex in band 9 contained the co-chaperones HAT1, RBBP7 and ASF1A-B along with H3 and H4. DNAJC9 was not detected, suggesting it does not form a complex with sNASP.

In summary, NASP forms distinct complexes containing either an H3 monomer or H3-H4 dimers, with monomeric H3 associating specifically with the s isoform. A sub-population of the NASP-H3 monomer pool is bound to the putative E3 ubiquitin ligase UBR7, previously shown to associate with H3 (41–43) and NASP (39, 44), whilst H3-H4 dimer-bound forms split into at least three complexes that differentially contain co-chaperones HAT1, RBBP7, ASF1A-B and/or the HSC70 family proteins HSPA1A, HSPA5 and HSPA8. Strikingly, we did not detect Imp5 in NASP-bound complexes despite it co-purifying with monomeric H3 (Fig.2D), suggesting that NASP and Imp5 form mutually exclusive complexes with histones.

Imp5 and sNASP are mutually exclusive in binding H3 and require RanGTP for hand-off.

We next investigated the interplay between Imp5 and sNASP binding. To prevent extraneous factors affecting our analysis, we used purified recombinant proteins reconstituted *in vitro*. Imp5 was able to bind equimolar concentrations of H3 and H4 when separated by size exclusion chromatography, demonstrating a direct interaction with histones, and interacted with both monomeric histones and H3-H4 dimers (Fig. S4A), as expected from its association with both WT and monomeric mutants (Fig. 2).

As sNASP and Imp5 elution overlapped in size exclusion chromatography (Fig.S4B), we used glycerol gradient ultracentrifugation to separate the two species (Fig. 4A & B). Purified Imp5-H3 complex was combined with an equimolar amount of sNASP and left to equilibrate for three hours on ice before separation. Interestingly, Imp5-H3 and sNASP eluted in separate fractions, suggesting direct competition for binding sites (Fig. 4B). In the reverse experiment where Imp5 was added to the NASP-H3 complex and equilibrated for 3 hours on ice, Imp5 was able to strip sNASP of its histone, with almost all H3 co-fractionating with Imp5 (Fig.S4D). This suggests that, firstly, as pre-assembled complex was used as input, NASP-H3 has a dissociation rate significantly below the incubation time for competition (three hours), secondly, Imp5 has a significantly higher dissociation constant than NASP towards monomeric H3, and thirdly, the dissociation of Imp5-H3 *in vivo* likely requires additional factors, such as release by RanGTP, rather than being mediated by direct competition.

To investigate this further, we purified bacterially expressed Ran and added it at equimolar concentrations to sNASP and Imp5-H3, allowing it to equilibrate for three hours on ice. In its purified state, which most likely represents the GDP-bound form, Ran was unable to bind to Imp5 and displace H3. To favour the GTP-bound state, Ran was incubated with 5 mM EDTA and 50 mM GTP for 20 minutes on ice (45), before performing the same competition experiment as above. Interestingly, RanGTP was bound to Imp5, displacing the majority of its H3 cargo, which was transferred to sNASP (Fig. 4D).

In summary, direct binding competition towards H3 likely represents the absence of complex formation between Imp5 and NASP that we see *in vivo*, with histone transfer mediated by the canonical RanGTP pathway.

Imp5 is the primary importin associated with H3 in the cytoplasm, whereas NASP binds only after nuclear import.

Both Imp4 (15–17) and Imp5 (17) have been shown to interact with H3-H4 in cytosolic extracts, with Imp4 being widely regarded as the primary import factor (7, 15–17). As cytoplasmic extracts often contain soluble nucleoplasmic proteins

DRAFT

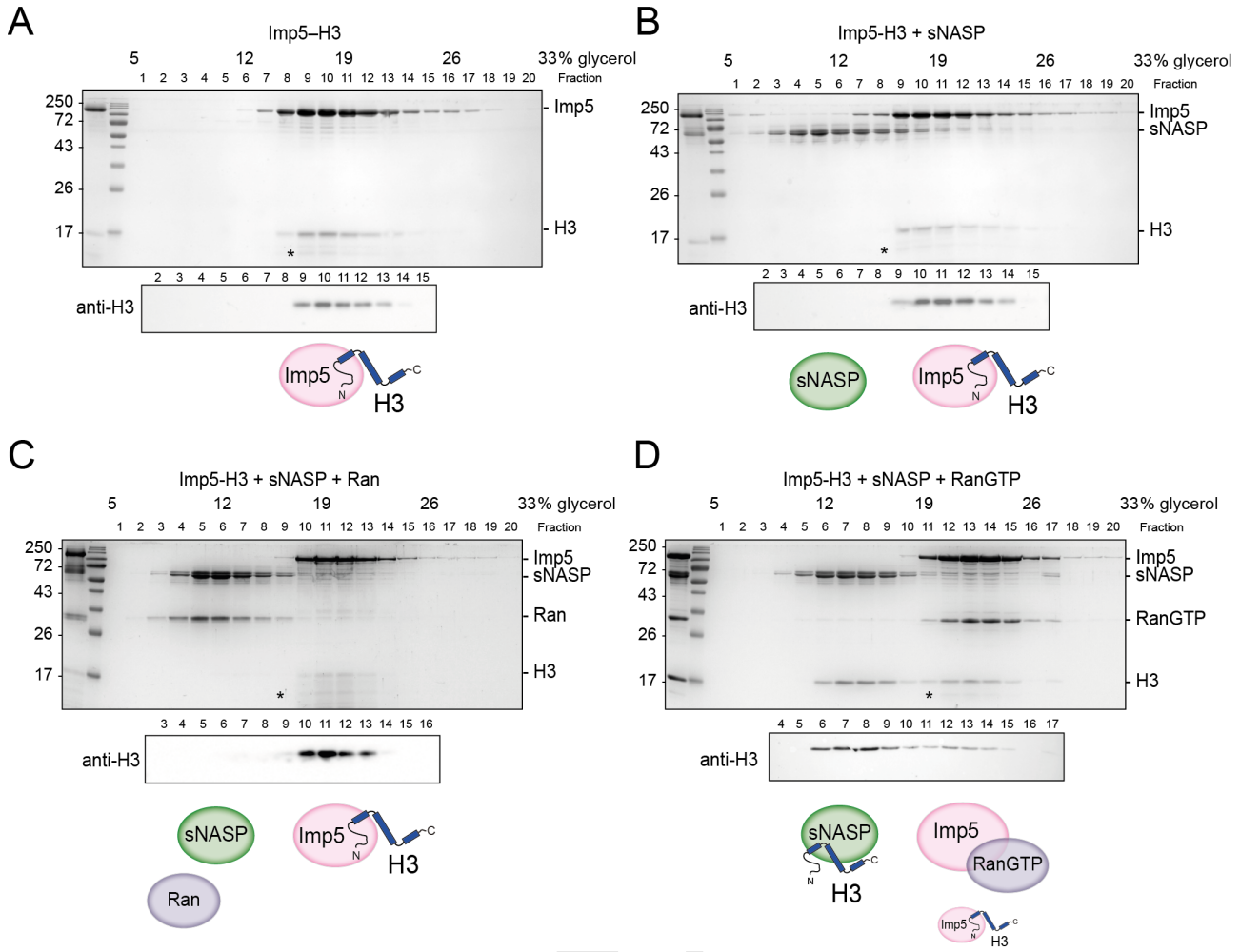

Fig. 4. H3 binding by Imp5 and sNASP is mutually exclusive and relies on RanGTP for histone transfer. A: Imp5-H3 reconstituted complex was purified by SEC and incubated on ice (control) for 3 hours before separating through ultracentrifugation on a 5-40% glycerol gradient. **B**: As in A, reconstituted complex was incubated on ice with equimolar concentration of sNASP (competition assay) for 3 hours before ultracentrifugation. H3 elutes with Imp5, whereas sNASP elutes in its separate fraction. **C**: As in B, but adding Ran in equimolar concentrations to sNASP and Imp-H3. Ran in its purified state is unable to bind to Imp5 and compete with H3. **D**: As in B, but adding RanGTP in equimolar concentrations to sNASP and Imp5-H3 complex. In this instance, RanGTP associates with Imp5 and displaces H3, which co-eultes with its chaperone sNASP. Asterisks indicate an Imp5 degradation product.

(21–23), we wanted to test interactions between H3, Imp4 and Imp5 *in situ* in living cells.

To do this we first employed mito-F2H (28) to probe their association using live-cell fluorescence microscopy. Mito-F2H builds on the principle of the F2H (Fluorescence 2-Hybrid) assay (46), but uses the outer mitochondrial membrane (OMM) as a cytoplasmic tether rather than an integrated LacO array in the nucleus (Fig. 5A). Using this technique, we previously demonstrated that tethered H3-eGFP was monomeric and associated with mCherry-Imp4 (21). To probe the interaction with Imp5, we co-expressed tethered eGFP with mCherry-Imp5 and quantified the colocalisation using Pearson's correlation coefficient (R). As expected, mCherry-Imp5 interacted strongly with tethered H3 at a level comparable to Imp4 (Fig. 5B and C), suggesting under conditions of over expression both importins can interact with cytoplasmic H3.

One drawback of mito-F2H is the static snapshot it gives of factors in the cytoplasm, whereas probing interactions dynamically as histones translocate to the nucleus would be more informative. To address this we used a previously developed pulse-chase method called 'RAPID-release' (Rapamycin Activated Protease through Induced Dimerisation and *release* of tethered cargo) (21). RAPID-release consists of two components: the histone cargo with a cytoplasmic tether localising to the outer mitochondrial membrane, and a protease that can be locally activated through rapamycin-induced recruitment (21). The system is highly adaptable and can be modified to study both localisation and interactions using appropriate functional tags such as fluorescent proteins and/or proximity ligation tags, such as APEX2 (Fig. 5D).

Firstly, to test the dynamic nature of Imp5's association with tethered H3, we released H3-mCherry in the presence of co-expressed eGFP-Imp5. The colocalisation observed under static conditions (Fig. 5C) disappeared when rapamycin was added to the cells, with H3 being imported rapidly and Imp5 remaining in the cytoplasm (Fig. 5E, top), as quantified by the reduction in Pearson's R value (Fig. 5E, bottom), suggesting that the Imp5-H3 interaction is cytoplasm-specific, and that hand-off to the nuclear chaperoning machinery is a

rapid event.

Secondly, to address which factors associate with tethered H3 proteome-wide, we incorporated an APEX2 tag into the tethered construct in a doxycycline-inducible FRT HeLa cell line. The APEX2 peroxidase allows for time-resolved, fast proximity biotinylation, requiring the xenobiotic biotin-phenol as a substrate and the addition of hydrogen peroxide for one minute as catalyser (47). Preliminary analysis showed that the APEX fusion presented slower release kinetics when compared to H3-eGFP alone, possibly due to the increase in steric hindrance derived from a considerably larger fusion construct, with the majority of tethered H3 being released 60 minutes after addition of rapamycin, and all being released by 120 minutes (Fig. 5F). We performed proximity ligation reactions at 0 min (cytoplasmic interactions), 10 min (mixed), and 120 min (nuclear interactions) after rapamycin addition allowing a one minute labelling window. Proximity ligation reactions were carried out in triplicate, quenched, and isolation of biotinylated peptides under denaturing conditions carried out. In this way, only interactions that occurred in the cell and not during post-lysis procedures were recorded.

The 0 min and 10 min datasets were very similar, owing to cleavage of the H3-eGFP-APEX2 tag being slower than the APEX2-free version (Fig. 5F, Fig.S5B and Table S4), restricting our analysis to 0 and 120 min, relating to cytoplasmic and nuclear interactions, respectively. To control for unspecific interactions, we filtered our results against a control comprised of tethered APEX without H3. Enrichment in the nucleus or cytoplasm was visualised in a volcano plot by plotting the LFQ ratio against a probability value derived from three biological replicates (Fig. 5G), with the triplicate LFQ scores for specific hits plotted individually alongside (Fig. 5H). Coloring hits based on their nuclear localisation, as determined by the human protein atlas (www.proteinatlas.org), revealed annotated cytoplasmic and mitochondrial proteins enriched at 0 min, and annotated nuclear proteins present at 120 min, as expected (Fig. 5G).

Both Imp4 and Imp5 were detected bound to H3 in the cytoplasm, but Imp5 was ∼100-fold enriched over Imp4 Fig. 5G & H) demonstrating that under endogenous conditions Imp5 is the primary importin associated with cytoplasmically tethered H3. NASP was only detectable after H3 had translocated to the nucleus, as were other known histone chaperones such as RBBP7-4 and MCM2 (Fig. 5G and H and Table S4), supporting our previous findings that NASP interacts with histones in the nucleus and not in the cytoplasm (21). Interestingly, we detected the HSC70 family member HSPA8, which bound to H3 comparably across the cytoplasm and the nucleus (Fig. 5G & H), suggesting a compartment independent role for this chaperone. Histone H4, as a common contaminant, was identified at similar levels across samples including the tethered APEX control, suggesting affinity for the tag or resin, and had to be excluded from analysis. In summary, (**?**) methods identify Imp5 as the major H3 binding importin (**?**), with NASP interacting with H3 only once it has translocated to the nucleus.

NASP binds rapidly to newly imported H3.

As the APEX2-tag suppressed the cleavage rate of tethered H3 in the RAPID-release assay we were unable to probe early events following H3 import. To address this we removed APEX and introduced the RAPID-release system into an eGFP-NASP CRIPSR cell line, swapping the H3-eGFP for H3-mCherry (Fig. 5A). Endogenously expressed eGFP-NASP was entirely nuclear, with no enrichment over the tethered histone, further showing they do not interact in the cytoplasm (Fig. 5B). Release of H3-mCherry by addition of rapamycin followed similar kinetics to previously described H3-EGFP (21), resulting in a half maximum cleavage at around 10 min (Fig.S6). Unlike Imp5 (Fig. 5E), association could not be inferred from the microscopy alone as H3-mCherry is diffuse in the nucleus after release similar to NASP. To address this, we performed co-IPs at 10 min, 1 hour and 24 hour intervals after histone release (Fig. 6C) to capture the interaction. Interestingly, H3 association with NASP peaked at the 10 minute time point, when the nucleus experiences the highest surge of the released histone (Fig. 6C, red arrows), strongly suggesting that NASP associates with H3 as it enters the nucleus. Association with H3 was also present at later time points, with 24 hours likely to represent an equilibrium between soluble and chromatin-bound state. This suggests that NASP can also interact with post-nucleosomal histone, and is not necessarily limited to the interaction with incoming, newly synthesised H3. Taken together, these findings suggest NASP is the predominant nuclear receptor for H3 monomer via a rapid hand-off event from Imp5.

Discussion

Rapid nuclear import and folding of histones is crucial for timely nucleosome deposition, funtionalisation and DNA safe-keeping. Several studies have identified Imp4 (16, 17, 41, 48–50), but also Imp5 (10, 17), as interacting with histones H3 and H4. In this study, we provide evidence that Imp5 is the primary importin bound to H3 when detected by *in situ* methods, and that, in contrast to Imp4, Imp5 interacts preferentially with a monomer of H3.

Due to the lack of structural information regarding Imp5's interaction with histones, it is not immediately clear why there is a functional difference in their binding. A recent structure of Imp4 in complex with H3-H4 and ASF1 (51) agrees with our finding that Imp4 does not interact with monomeric H3 and H4 mutants, in that, although Imp4 interacts predominantly with the N-terminal region of H3, it also makes contacts with the histone fold domain of H4. This is in contrast to Imp9's interaction with its H2A-H2B cargo, where it fully encapsulates an H2A-H2B dimer (14). Thus, whilst a divergent histone interaction between Imp4 and Imp5 should not be ruled out, it seems likely that Imp5 binds to H3 and H4 in a similar way as Imp4, but potentially with more emphasis on the H3 N-terminal region, having lost the necessity for an H3-H4 dimer substrate.

Imp5 binding to H3 precludes NASP interaction, both in proteomic analyses and in *in vitro* binding experiments, with the nuclear localisation of NASP suggesting NASP acts down-

DRAFT

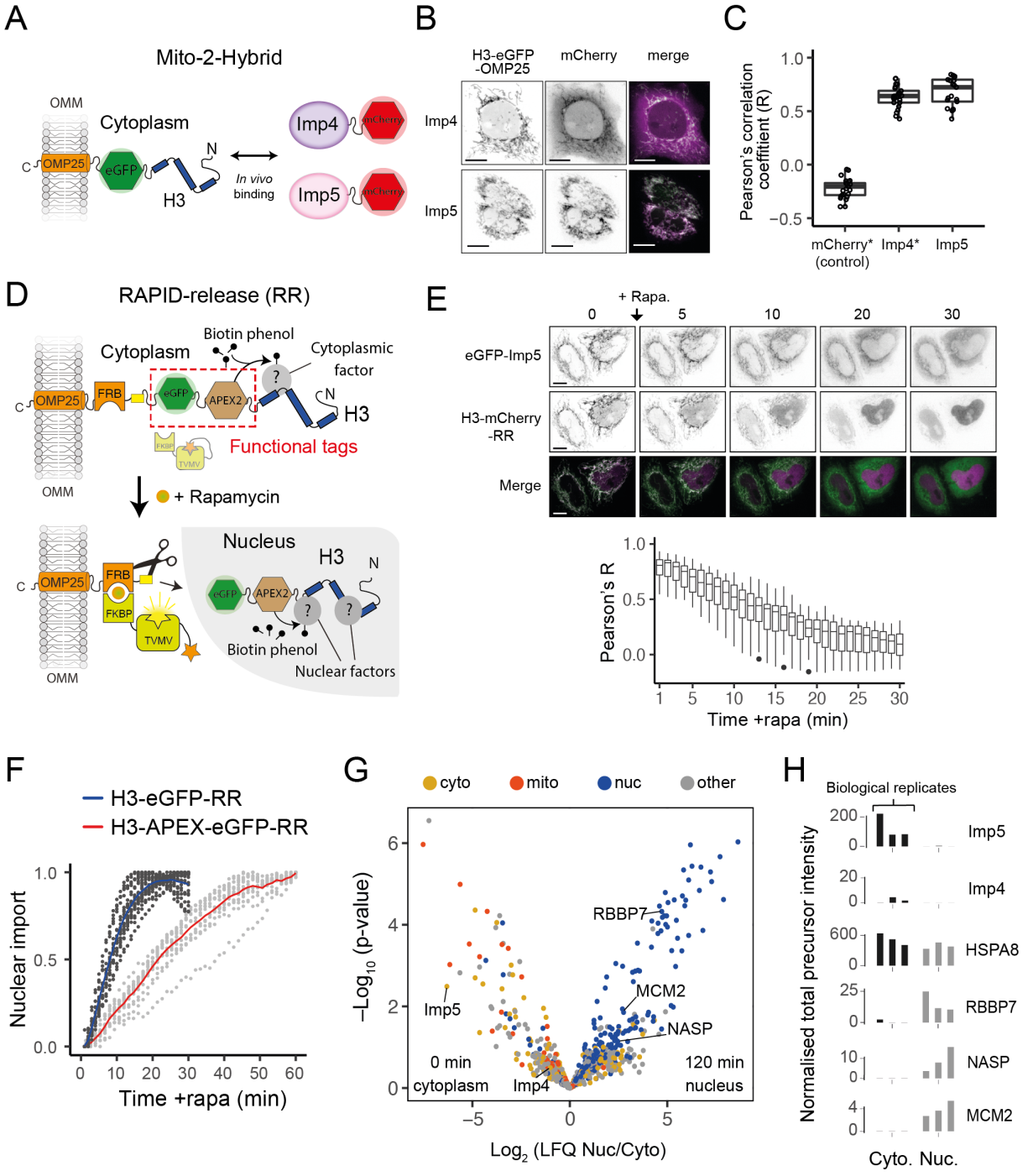

Fig. 5. Imp5 is the predominant importin bound to nascent H3 in the cytoplasm, with histone chaperones binding only after nuclear import A: In the Mito-2-Hybrid assay cytoplasmic interactions are detect by tethering of a bait protein (H3) to the outer mitochondrial membrane (OMM) via an OMP25 tail-anchoring peptide. Recruitment of a co-expressed soluble protein reports an interaction with the bait. Scale bar = 10 µm. **B**: Representative images of Imp4 and Imp5 interaction with tethered H3. **C**: Quantification of interactions shown in B using the Pearson's correlation coefficient as a measure of colocalisation. Asterisks indicate plotting of previously published values (21). **D**: Experimental design for incorporating RAPID-Release (RR) into the cytoplamsmically tethered H3 contruct. Functionalisation is introduced by adding required tags to the tether (top, examples in this case being eGFP and APEX2), which can be released along with the cargo (H3) to study interaction dynamics after the addition of rapamycin (bottom). **E**: Imp5 dissociates from H3 as it is released from its tether and enters the nucleus, suggesting a rapid hand-over mechanism. **F**: Nuclear import rate of H3.1-eGFP and H3.1-APEX-eGFP. Single cells are represented as grey dots. Averages are highlighted as blue (H3.1-eGFP) and red (H3.1-APEX-eGFP). Note, H3.1-eGFP nuclear import plateaus within 20 minutes whereas H3.1-APEX-eGFP requires up to 60 minutes. **G**: Volcano plot representing label-free mass spectrometry quantification analysis (LFQ) after streptavidin pull-down of proximity labeled proteins at 0 min (cytoplasm) or 120 min (nucleus) post rapamycin addition. Interacting factors are colour-coded according to their main subcellular location: cyotoplasm (cyto) yellow, mitochondria (mito) orange, nucleus (nuc) blue and other in grey (The Human Protein Atlas version 21.1). **H**: Alternative representation of proteomics data showing quantitative values (normalised total precursor intensity) on a linear scale ($1x10^6$) for each biological replicate of key factors identified in F.

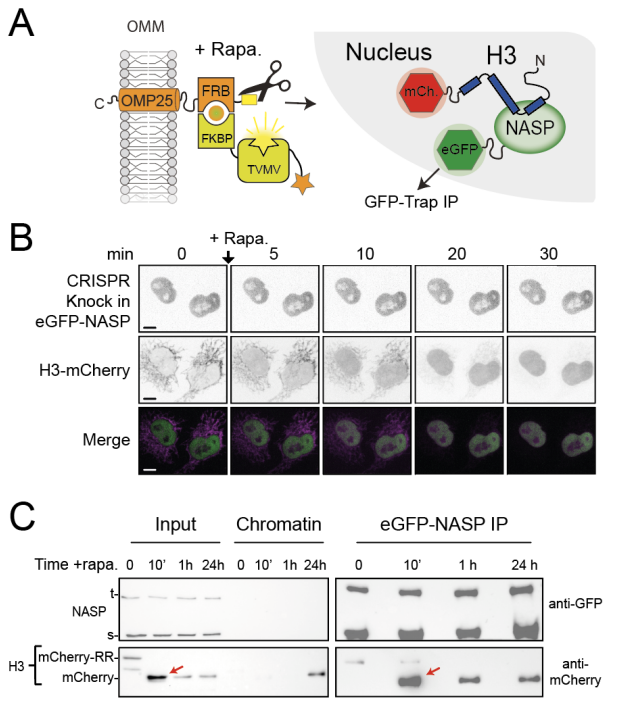

Fig. 6. NASP binds rapidly to newly imported H3 A: Experimental design combining a histone pulse with co-immunoprecipitation. Addition of rapamycin recruits an otherwise auto-inhibited TVMV protease which cleaves the tethered histone fusion allowing it to enter the histone deposition pathway. **B**: Time course of H3-mCherry release in the CRISPR eGFP-NASP knock in cell line. Note, endogenously tagged NASP does not associated with H3 tethered in the cytoplasm. **C**: Western blot analysis of co-immunoprecipitated H3-mCherry from the cell line shown in B at 0, 10 min, 1 h and 24 h time points after the addition of rapamycin.

stream of Imp5 in the histone chaperoning pathway. The TPR domain of NASP has two distinct interaction sites with histone H3: an H3 N-terminal binding surface and an H3α3 binding pocket (28–31). Overlapping binding sites likely explains the H3 N-terminal competition between importin and chaperone that we see, however, if this were the only Imp5 interaction site one might expect NASP to remain bound through the H3α3 (28, 29). Additional interactions between imp5 and the histone fold domain of H3 could be one explanation for the lack of trimeric complex. Alternatively, H3α3 binding by NASP may be more complex and require additional factors. In either case, we show it is RanGTP that provides the switch necessary for release of H3 from the importin, which is in contrast to Imp9-H2A-H2B, where RanGTP alone was insufficient (14), highlight further diversity amongst importin-β proteins and their handling of histones.

If newly synthesised H3 and H4 are rapidly imported into the nucleus as monomers bound to Imp5, what is the role of the long-established Imp4-H3-H4-ASF1 complex? One explanation is that Imp4 recognises post-nuclear H3-H4-ASF1, promoting the re-import of H3-H4 dimers that may have escaped. Indeed, the H3-H4-ASF1 complex could be small enough to transit the nuclear pore passively (52), with ASF1, unlike NASP, not containing a nuclear localisation sequence. Furthermore, pure cytosolic extracts without nucleoplasmic leakage are difficult to obtain (22, 23, 53), further promoting the appearance of H3-H4-ASF1 in the cytosol. To compound this, ss nuclear import of histones occurs rapidly after synthesis, the small pool of Imp5-associated histones present at any one time is likely obscured in these biochemical analyses.

The necessity to sequester monomeric histones in the nucleus may relate to the folding kinetics of H3-H4. *In vitro* studies suggest that H3-H4 folding is the rate-limiting step in the dimerisation pathway (54), with a milisecond timescale comparable to that of nuclear pore transit (55, 56). NASP may therefore be regarded as having a 'holdase' function, as has been suggested for the ATP-independent small heat shock protein family of molecular chaperones (57–62), preventing aggregation of H3 in the nuclear milieu before encountering H4. It is interesting that it is specifically sNASP rather than tNASP that co-separates with the H3 monomer, suggesting alternative functions for these two splice isoforms. tNASP incorporates exon 8 that functionally extends the acidic region of sNASP. How this insertion mediates the differing binding profiles we see would be an interesting future question. The role of NASP as a holdase is easily reconciled with the idea of NASP overseeing a reservoir of soluble histones (27, 63), which would be compatible with its acting in the nucleus. In addition, the presence of NASP in downstream complexes (16, 19), mediated by interactions outside of the TPR-H3 peptide interface (29–31), supports NASP guiding the transition from monomeric import to a heterodimer capable of DNA deposition (31).

The holoenzyme HAT1-RBBP7's interaction with monomeric H4 mutants suggests that HAT1-RBBP7 may function as a counterpart to NASP-H3, accepting H4 from Imp5 in the nucleus prior to folding. In support of this, structural characterisation of the homologous Hat1p-Hat2p complex from yeast suggests that dimerisation with H3 is not necessary for interaction with H4, which is mediated predominantly with the H4 tail and α1 region (64). The HAT1-RBBP7 complex is responsible for H4K5Ac and H4K12Ac on newly synthesised histone H4 (65). Interestingly, in NASP pulldowns we find histone H4K5Ac peaking in bands with sparse HAT1, suggesting a catalytic turnover of HAT1, but with retention of RBBP7, which may be related to its interactions with H3 N-terminal tail (66). The low levels of ASF1 detected in complex with HAT1 is notable and suggests a transitory state, potentially involving competition between the TPR domain of NASP and ASF1 for the H3$alpha$3 helix (29, 34, 35).

Unexpectedly, we found the ubiquitin ligase UBR7 co-migrating with a NASP-H3 monomer peak. UBR7 associates with H3 and its centromeric homolog CENP-A (41–43, 67), with proposed interactions occurring between its PHD finger domain and the methylated tail of H3 (42). Additionally, UBR7 is also responsible for H2BK120-directed monoubiquitin ligase activity (68). The function of UBR7 in the context of soluble H3 is less clear, and need not relate directly to the major function of the NASP-H3. Indeed, UBR7 co-migrated with sNASP and H3 in native PAGE, but did not fractionate with sNASP-H3 after glycerol gradient centrifugation, suggesting a distinct subcomplex population (Fig.

DRAFT

3). According to our label-free quantification, UBR7 was roughly one order of magnitude lower than the NASP-H3 pool, further suggesting it may have a secondary role in histone metabolism, potentially related to histone degradation (27, 63) or redeposition (39).

With regards to integration with the heat-shock protein folding machinery, we observe interactions with different HSC70-type chaperones, namely HSPA8, HSPA1A-B and HSPA5. Intriguingly, HSPA8 forms a complex with NASP and H3-H4 which is distinct from other co-chaperoning complexes, perhaps relating to the degradation of misfolded histones, as previously proposed (27, 63). Their cross-compartment binding could also relate to the folding or refolding of aggregated histones, as recently suggested for the HSP70 recruitment factor DNAJC9 (32). We did not detect DNAJC9 associating in a co-chaperoning complex with NASP, which, along with DNAJC9's recognition of an H3-H4 dimer, may suggest DNAJC9 acts after NASP binding or in a parallel pathway for aggregated or misfolded dimers. We also detect the new histone chaperone C1QBP (40) bound to monomeric mutants of both H3 and H4. However, we do not see association with NASP, suggesting a potential upstream function of this protein. The role of these novel histone-binding factors in the histone chaperoning pathway will require further analyses to reveal their function in detail.

In summary, we propose a model in which monomeric H3 and H4 are imported into the nucleus via an Imp5-dependent pathway (Fig. 7). In this model, H3 and H4 are transferred to NASP and HAT1-RBBP7, respectively, dimerising in the nucleus rather than the cytoplasm. The ability to form stable nuclear pools of monomeric histones would provide an additional level of contingency for counteracting imbalances in histone supply, enabling a soluble reservoir of histone to be maintained under adverse cellular conditions.

Unexpectedly, we found the ubiquitin ligase UBR7 capable of interacting with monomer H3. UBR7 has been previously implicated with chromatin processes. UBR7 associates with H3, and its centromeric homolog CENP-A, (41–43, 67), with proposed interactions occurring between its PHD finger domain and the methylated tail of H3 (42). Additionally, UBR7 is also responsible for H2BK120 directed monoubiquitin ligase activity (68). The function of UBR7 in the context of soluble H3 is less clear, and need not relate directly to the major function of the NASP-H3. Indeed, UBR7 was in same native fraction as NASP and H3, but not so in the glycerol gradient fractions suggesting a distinct subcomplex population (Fig. 3). According to our label-free quantification UBR7 content was roughly one order of magnitude lower of that of the NASP-H3 pool, suggesting it may have a secondary role in histone metabolism, potentially related to histone degradation (27) (Hormazabal 2022 10.1093/nar/gkab1296 or redeposition (Hogan 2021). Similarly, we detect the new chaperone C1QBP (40) bound to monomeric mutants of both H3 and H4 at similar levels to UBR7. However, we do not see association with NASP, suggesting a potential upstream function of this protein. The role of these novel histone-binding factors in the histone chaperoning pathway will require further analyses to reveal their function in detail.

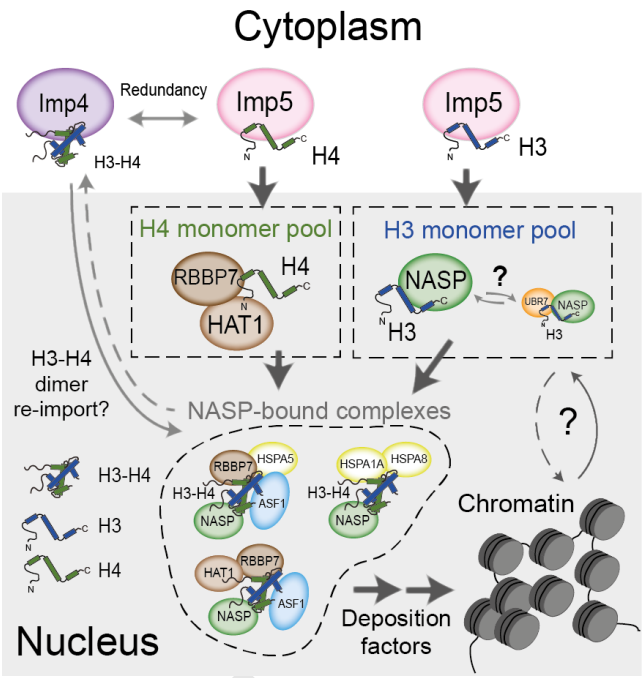

Fig. 7. Model for nuclear translocation of histones H3 and H4 as monomers and processing in the nucleus Imp5 imports histone H3 and H4 as monomers whilst Imp4 has a preference for dimers, albeit with some redundancy. Upon nuclear translocation, RanGTP induces cargo dissociation with H3 being transferred to sNASP and H4 to the HAT1 complex. These chaperones may have a holdase function that buffers imbalances in individual histone supply. H3 and H4 fold and enter the deposition pathway via a number of distinct NASP-bound complexes

The holoenzyme HAT1-RBBP7 interaction with both monomer histone H4 mutants suggests that HAT1-RBBP7 may function as a counterpart to NASP-H3, accepting H4 from Imp5 in the nucleus prior to folding. In support of this, structural characterisation of the homologous Hat1p-Hat2p complex from yeast suggests that dimerisation with H3 is not necessary for interaction with H4, which is mediated predominantly with the H4 tail and $\alpha 1$ region (64, 66).

The HAT1-RBBP7 complex is responsible for lysine K5 and K12 acetylation in newly synthesied histone H4 (65). Interestingly, in native isolation of NASP-associated complexes, we find histone H4 K5 acetylation peaking in bands with sparse HAT1 (Fig. 3), suggesting a transition from an earlier sub-complex of NASP-RBBP7-HAT1 where the catalytic activity may take place. The retention of RBBP7 could be related to the interactions with H3 N-terminal tail (Yue 2022, 10.1101/gad.349099.121). The low levels of ASF1 detected in complex with HAT1 is notable and may allude to transitory state in which the TPR domain of NASP is still engaged with the C-terminal region of H3 which is necessary for ASF1 binding to H3-H4 (34, 35). Future research unraveling the details, structural and temporal, of these transitions will be of great interest in the field.

In summary, we propose a monomeric histone supply pathway for H3 and H4 fed by the importin Imp5 that transfers histones to NASP and HAT1-RBBP7, respectively. In this model, NASP and HAT1-RBBP7 provide a buffer function for monomer histones that smooths imbalances in histone

DRAFT

production, elude the requirement for cytoplasmic folding and provide an environment for dimerisation local to the assembly of the H3-H4 heterodimer.

Materials and methods

Cloning and plasmid material.

Plasmids were constructed through cloning PCR, annealed oligo ligation, gBLOCK synthesis (IDT™) and Gibson assembly (69). All constructs were verified by Sanger sequencing. The open reading frame from Imp5 isoform 1 (Uniprot identifier: O00410-1) was amplified from HeLa cDNA and ligated into pEGFP-C1. For bacterial protein expression Imp5, was re-cloned into pGEX-6P1 (Cytiva). $(His)_6$-sNASP, H3 and H4 histones constructs have been detailed previously (28, 31). The RAPID-release plasmids were used as previously published (21). In order to contain the 2-component RAPID-release system in a single vector the tethered cassette (H3.2mCherry-TVMVcsx2-FRB-OMP25) and the protease cassette (FKBP12-TVMV-AI) were cloned either side of an Internal Ribosome Entry Site (IRES). CRISPR knock-in cell lines were obtained following the D10ACas9 nickase using the paired guide RNAs protocol (70). For the Homologous DNA Repair (HDR) template, 800 bp upstream and downstream of the start codon were amplified from genomic DNA, and ligated through Gibson assembly to EGFP and mCherry, respectively, so that an in-frame 5' fusion to exon 1 was formed. This was cloned into pBlueScript II KS (+) as destination plasmid. Guide RNAs were prepared as described, combining two complementary oligonucleotides into D10ACas9 vector pX461-PSPCas9N(BB)-2A-GFP (Addgene #48140). For the inducible expression of H3-APEX-GFP, APEX2 was inserted between the H3 and GFP cassettes in the RAPID release vector pH3-eGFP^{TVMVcsx2}-FRB-OMP25 (21), and subcloned into pcDNA™FRT/TO (Thermo) plasmid for recombination in the HeLa Flp-In™ T-REx™ system. See plasmid sequences in Table S1 and primer sequences and DNA fragments in Table S2 for details.

Protein expression and purification.

All recombinant proteins were produced in Rosetta2 *Escherichia coli* competent cells (Thermo Fisher) induced with 0.4 mM isopropyl-β-d-1-thiogalactoside (IPTG) at an OD_{600} of 0.6, unless otherwise stated. sNASP was expressed overnight at 21 °C as an N-terminal $(His)_6$ fusion construct and purified using Ni-NTA affinity resin (Cytiva) and further purified by ion-exchange chromatography after cleavage of the $(His)_6$ fusion by TEV protease as previously described (28).

Importin-5 (Imp5) purification was addapted from (18). Briefly, GST-Imp5 construct was induced for 12 hours at 24 °C. Bacteria were pelleted and lysed in 50 mM Tris, pH 7.5, 150 mM sodium chloride, 20% glycerol, 2 mM dithiothreitol, 1 mM EDTA, protease inhibitors and lytic cocktail (10 μg/mL RNase A, 100 μg/mL DNase I, 1 mg/mL Lysozyme) for 2 hours at 4 °C, followed by flash-freezing in liquid nitrogen. Pellets were rapidly thawed at 37 °C and quickly placed on ice before sonication with a Misonix sonicator (3 pulses 'on' for 10 seconds and 'off' 30 seconds with an amplitude of 25). Imp5 was then purified with GST-trap resin (Cytiva) and further purified by anion-exchange chromatography following overnight cleavage wih 3C protease.

Ran purification was performed as previously described, (71). Ran was GTP loaded at 10x final concentration for competition essays, with 50 mM GTP in 5 mM EDTA 50 mM HEPES pH 7.5 on ice for 30 min.

Full length *Xenopus laevis* histones H3 and H4 were purified and refolded as previously described (72).

Analytical gel filtration.

Analytical gel filtration was carried out using a Superdex Increase 200 10/300 column (GE Healthcare) in 20 mM HEPES-KOH pH 7.5 and 150 mM sodium chloride, unless otherwise stated. 0.6 ml fractions were collected encompassing the void and bed volumes of the column. Proteins and complexes were reconstituted at a concentration of 20 μM. Fractions were separated by SDS-PAGE and stained with Coomassie Brilliant Blue (Instant Blue®, Abcam).

Competition assay.

Purified Imp5 or sNASP were mixed with equimolar amount of histone H3 (20 μM final concentration) in 20 mM HEPES-KOH pH 7.5, 150 mM sodium chloride, 2 mM magnesium acetate, 1 mM EGTA, 2 mM dithiothreitol and 10% glycerol and allow to equilibrate for 10 min on ice before spinning at 20,000 g for 20 min at 4 °C to remove any precipitate. Complexes were isolated on Superdex Increase S200 10/300 column (GE Healthcare) and central fractions were pooled, concentrated with a 10 kDa concentrator, before competition. Preformed Imp-H3 and sNASP-H3 complexes were combined with an equimolar amount of sNASP or Imp5, respectively, with or without the addition of Ran and GTP loaded Ran (RanGTP) and left to equilibrate for three hours on ice before separation on a glycerol gradient.

Glycerol gradient ultracentrifugation.

Adapted from (73). Briefly, protein mixtures were diluted to 6.25 μM in 200 μL of gradient loading buffer (20 mM HEPES pH 7.5, 150 mM sodium chloride, 2 mM dithiothreitol, 1% glycerol and 5 mM GTP for the RanGTP samples) and gently layered on a 5 mL gradient of 5–40% glycerol (20 mM HEPES pH 7.5, 150 mM sodium chloride, 2 mM dithiothreitol 5 or 40% glycerol and 5 mM GTP for the RanGTP samples) made with Gradient Master (BioComp): Program Short Glycerol 5-40%. The samples were spun on a pre-chilled Optima XPN-80L ultracentrifuge (Beckman Coulter), rotor Sw55Ti, at 240,000 g for 14 hours at 4 °C. 200 μL fractions were manually collected, and separated by SDS-PAGE for Coomassie staining (Instant Blue®, Abcam).

Tissue culture and cell lines.

HeLa Kyoto cells (originally sourced from CRUK Cell Services, and cultured in house) were grown to 70% confluency in DMEM-Hi glucose (Gibco) supplemented with 10% heat-inactivated foetal bovine serum (Sigma), 50 μg/ml penicillin/streptomycin at 37°C in a humidified incubator

DRAFT

with 5% CO_2. Cells were passaged with 0.25% trypsin-EDTA and resuspended in complete media. Cells were transfected following the Fugene® HD manufacturer's instructions (Promega) and imaged imaged 24-48 hours post-transfection.

For stable lines, HeLa or HeLa FRT cells were transfected as described above. After 48 hours antibiotic selection was performed and cells and split when required. After 14 days the transfection was sorted into fluorescent-positive single cells through flow cytometry.

For HEK293-F expression, cells were grown in suspension to $1x10^6$ cells/mL with serum-free FreeStyle 293 expression medium (Thermo Fisher), supplemented with 25 μg/ml penicillin/streptomycin, in a humidified incubator with 8% CO_2 and 120 rpm. HEK293-F cells were split 24 hours before transfection to $0.5x10^6$ cells/mL, and transfected with 1 μg of DNA per $2x10^6$ cells and 3 μg of linear PEI per 1 μg of DNA in OptiMEM (60 μL per 1 μg of DNA), vortexed briefly and incubated at room temperature for 15 min before adding to the cells.

CRISPR knock-in cell lines.

CRISPR knock-in cells were obtained following the established protocol (70). Briefly, for HeLa cell lines, cells were co-transfected with plasmids encoding upstream and downstream sgRNA, the D10ACas9 nickase and the HDR template on 6-well plates at 70% confluency using FuGene® HD (Promega). Cells were allowed to recover for 7-10 days (splitting if necessary) before single clone selection through flow cytometry. For HEK293-F CRISPR knock-in populations, 10 mL of cells at a $1x10^6$ cells/mL confluency and transfected with the same CRISPR plasmids as for HeLa cells following the transfection protocol for HEK293-F in suspension as described above. After 7 days ((splitting when required) cells were FACS to collect $\tilde{1}x10^6$ cells, allow to recover for 15 days and FACS again for purity $\tilde{1}x10^6$ cells.

Flow cytometry.

Single HeLa, HeLa FRT and HEK293-F cells were sorted with a BD FACSAria™ Fusion Flow Cytometer, using a 100 μm nozzle, gating FSC-A/FSC-H for singlets and laser compensation using negative and positive controls. HeLa and HeLa FRT cells were harvested by incubation with trypsin-EDTA for 5 min as before, and rinsed in PBS twice by centrifugation at 200 g for 5 min at 4 °C. Cells were then resuspended in phenol red-free DMEM supplemented with 2% FBS, filtered through a 50 μm Cell Strainer cap (Falcon) and sorted into 96 well plates with 1000 μL 1:1 fresh DMEM:conditioned DMEM (from pre-sorted medium) supplemented with 20% FBS. HEK293-F cells were resuspended in fresh FreeStyle 293 medium and sorted for yield. Sorted cells were rinsed in PBS twice by centrifugation at 300 g for 5 min at 4 °C. Final media contained 1:1 fresh:conditioned (from pre-sorted) medium.

Cell fractionation.

Cell fractionation was performed following the REAP protocol (74) as previously adapted by (21). Either cells on plates or cells in suspension were washed twice with PBS before collection. Cells on suspension were pelleted at 200 g, 5 min, 4 °C between washes. Adherent cells were scraped into ice-cold PBS and pelleted the same way before resuspension in lysis buffer (0.1% NP-40 in PBS containing the protease inhibitors PMSF, aprotinin, leupeptin, pepstatin and benzamidine). Lysis was continued for 10 min on ice, before pelleting of the chromatin fraction for 10 min at 1,000 g 4 °C. The supernatant was again spun at 2,000 g 4°C, and then removed to a fresh tube and spun for 20 min at 20,000 g to remove cell debris. For Co-IP experiments, in order to ensure identical loading across samples, the amount of GFP-bound protein was assessed by loading final extract in sample buffer (without boiling) on a Mini-PROTEAN TGX Precast Gel (BioRad), visualised with LED_{488} illumination (G-box, Syngene) and quantified against recombinant GST-eGFP using ImageJ software (Fig.S1).

Immunoprecipitation.

Soluble cell fractions were bound to 10 μL per mL of lysate of GFP-Trap® (ChromoTek™) agarose beads. Binding was allowed to proceed for 1 hour at 4°C with continual nutation. Beads were spun for 2 min at 250 g, 4 °C and washed once in 20 mM Tris–HCl pH 7.5, 400 mM sodium chloride and 0.1% NP-40 (high salt buffer), followed by three washes in PBS + 0.1% NP-40, and one last wash in PBS. For SDS-PAGE analysis, the beads were either boiled directly in 2xLaemmli sample buffer. For 1D Native PAGE, the beads were incubated in PBS 2 μM dithiothreitol, at 4 °C for 16 hours with TEV protease to release bait complexes. For mass spectrometery, the beads were washed four times with 50 mM ammonium bicarbonate, alkylated in 10 mM TCEP, 40 mM CAA in 50 mM ABC for 5 min at 70 °C and incubated with 1 μg Trypsin per 100μg protein and digested at 37 °C overnight.

Glycerol gradient ultracentrifugation.

After overnight TEV cleavage, soluble samples were separated from GFP-trap matrix by filtration through 0.22 μm nilon filter (Co-star) spun at 2,000 g for 2 min at 4 °C before directly loading on a glycerol gradient for separation (73). on As described above, IP extracts were gently layered on a 5 mL gradient of 4–20% glycerol (20 mM HEPES pH 7.5, 150 mM sodium chloride, 2 mM dithiothreitol) made with Gradient Master (BioComp): Program Short Glycerol 5-25% w/v. The samples were spun on a pre-chilled Optima XPN-80L ultracentrifuge (Beckman Coulter), rotor Sw55Ti, at 240,000 g for 14 hours at 4 °C. 200 μL fractions were manually collected, and separated by SDS-PAGE for Coomassie staining (Instant Blue®, Abcam) and western blot analysis.

Native gel (1D) and 2D gel separation.

After overnight TEV cleavage, soluble samples were separated from GFP-trap matrix by filtration through 0.22 μm nilon filter (Co-star) spun at 2,000 g for 2 min at 4 °C. Protein complexes were concentrated to 25 μL in 30 kDa centrifugal concentrator (Vivaspin 500 Sartorius) and mixed with equal volume of 2 x native gel sample buffer (62.5 mM Tris-HCl, pH 6.8, 40% glycerol, 0.01% bromophenol blue) (BioRad).

DRAFT

Three lanes were loaded on a 4-20% polyacrylamide Mini-PROTEAN TGX Precast Gel (BioRad) and run with 25 mM Tris, 192 mM glycine, pH 8.4 buffer. The gel was run for 6 hours below 10 mA (20 min at 20 V, 30 min at 30 V, 60 min at 60 V, 120 min at 120 V and 120 min at 160 V). The gel lanes were longitudinally cropped, using one of them for Coomassie staining, from which bands were cut and stored at -80 °C until mass-spectrometry analysis. Gel bands were in-gel digested according to (75). The other two lanes were incubated with 1xTris/glycine/SDS buffer for 15 min and then incubated with 2 x Laemmli sample buffer (BioRad) for 15 min, heated twice for 15 seconds in the microwave (800 mA) and loaded on 15% polyacrylamide gel for 2D separation. One gel was dedicated to Coomassie staining and the other one was used for western blot analysis.

Western blot analysis.

SDS-PAGE gels were transferred onto a nitrocellulose membrane using an iBlot 2 Dry Blotting System (Thermo Fisher), blocked with 3% powdered milk in TBS-T and then incubated at 4°C overnight with primary antibodies diluted in 3% powdered milk or 3% BSA. Antibody dilutions were made at 1:1,000 ratios except anti-NASP (21), which was diluted to 1:10,000-40,000). Membranes were washed with TBS-T and then incubated for 1 h at room temperature with the HRP-conjugated secondary antibody. See Table S3 for list of antibodies.

APEX biotinylation and sample preparation.

Proximity biotinylation was performed according to (47). Briefly, per condition, four 15 cm^s plates were induced for 24 hours with 0.5 μg/mL doxycycline. Rapamycin (200 nM final) was added 120 min before harvesting to release histone H3-APEX2-EGFP, compared to mock-treated cells (time 0). Thirty minutes before harvesting, cell media was supplemented with biotin-phenol (Iris Biotech) to final concentration of 500 μM and incubated for 30 min at 37 °C 5% CO_2, before 200 μL per 15 cm plate of 100 mM H_2O_2 (final concentration 1 mM) was added and incubated for 1 min at room temperature with gentle shaking (100 mM stock was prepared from fresh H_2O_2 Merck 30% w/w).

The reaction was quenched by washing cells three times with ice-cold 5 mM trolox, 10 mM sodium ascorbate, 0.03% sodium azide in PBS. Cells were scraped off the plates and lysed with RIPA lysis buffer (50 mM Tris-HCl, pH 7.5, 150 mM sodium chloride, 0.1% SDS, 0.5% sodium deoxycholate, 1% Triton X-100, protease inhibitors (as detailed above) and 2 μL benzonase (Sigma)) for 20 min on ice. Lysates were clarified by centrifugation at 16,000 g for 10 minutes at 4 °C before protein concentration was determined by Bradford assay. 25 μL of Pierce™ High Capacity Streptavidin Agarose (Thermo Fisher) was used for each condition. Lysates of equal protein concentrations were incubated with streptavidin beads for 60 min at 4 °C , washed twice with cold lysis buffer, once with cold 1 M KCl, once with cold 100 mM sodium carbonate, once with cold 2 M urea in 50 mM ammonium bicarbonate and three times in 50 mM ammonium bicarbonate.

Samples were alkylated in 10 mM TCEP, 40 mM chloroacetamide in 50 mM ammonium for 5 min at 70 °C and digested with 1 μg trypsin per 100μg protein 37 °C overnight. The pH was adjusted to 3.5 before peptide storage at -20 °C.

LC-MS/MS and data analysis.

Peptides from on-gel digestion or on-beads digestion were analysed on a Orbitrap Fusion with UltiMate 3000 RSLC-nano System (Thermo Scientific). The raw data were searched using MaxQuant software (Version: 1.6.10.43) against UniProtKB Human database and the common contaminants database from MaxQuant (76) from peptides generated from a tryptic digestion.

The software Scaffold (TM, Version: 4.8.9, Proteome Software Inc.) was used to validate MS/MS-based peptide and protein identifications. With the exception of BioID experiments, peptide identifications were accepted if they could be established at 95% probability or higher by the Scaffold Local FDR algorithm. Protein identifications were accepted if they could be established at 99% probability or higher and contained at least two identified peptides. For BioID experiments thresholds were 95% for peptide identification, 95% for protein identification. Proteins that contained similar peptides and could not be differentiated based on MS/MS analysis alone were grouped to satisfy the principles of parsimony. Proteins sharing significant peptide evidence were grouped into clusters. For the histone mutant experiments, since the data was very robust with strong signal, normalised total precursor intensity for proteins or protein clusters containing that were not identified in all 3 replicates of at least one condition (WT and the two mutants), were filter out. Next 0 values were replaced with a fix value below detection limit, arbitrarily assigned to 1/2 of the lowest detected value. The $\log_2$ of these values were normalised with 'scale' Limma package normalisation and used to build a linear model (77) from which adjusted p-values (FDR) were obtained for pairwise comparisons (Table S4). For the native gel protein identification, ANOVA analysis was performed in R with adjusted p-values (FDR), (Table S4). For the BioID experiments, containing more protein hits and far more 0 values than the affinity-purified experiments, were processed with DEP package (Zhang 2018, 10.1038/nprot.2017.147) for data normalisation and imputation with the parameters ("MinProb" q = 0.01), recommended for samples with numerous missing values (Table S4), from which a linear model with Limma using DEP directly.

The mass spectrometry proteomics data have been deposited to the ProteomeXchange Consortium via the PRIDE (78) partner repository with the dataset identifier PXD029354 and 10.6019/PXD029354.

Imaging.

All images were captured using an UltraVIEW VoX Live Cell Imaging System (PerkinElmer) with a 37°C environmental chamber. Cells were cultured in 8-well μ-slides (ibidi) with 200 μL Leibovitz's L-15 (L-15) medium (Thermo Fisher Scientific) supplemented with 4 mM l-glutamine and 50 μg/ml penicillin/streptomycin. For DNA staining, cells were

DRAFT

stained with 1 μg/ml Hoechst for 10 min before washing with PBS and restoration of L-15 medium.

For RAPID-release experiments, L15 medium containing 1 μM rapamycin was added directly to the well resulting in a final concentration of 200 nM rapamycin. An initial image stack was taken prior to rapamycin addition, serving as time 0, after which cells were imaged every minute for up to 30 min.

For RAPID-release of tethered H3.1-mCherry and soluble eGFP-Imp5, cells were co-transfected with H3.1-mCherry-RR and EGFP-Imp5 with release being performed as described above, allowing H3.1 and Imp5 to be followed in the red and green channels, respectively. For RAPID-release of tethered H3.1-mCherry and endogenous EGFP-NASP a stable cell line was used.

Partitioning and quantification of the images was carried out using ImageJ. Z-stacks spanning the cell were flattened into a maximum pixel intensity image. The cytoplasm and nucleus were manually partitioned for each cell, and the nuclear enrichment over the cytoplasm was calculated for each time point. Values for individual cells were normalised between 1 and 0 and plotted on the same axes for comparison.

The Pearson's correlation coefficients for Mito-2-hybrid (M2H) between the mCherry and the eGFP channels were calculated at each time point using the ImageJ were calculated using the GDSC Colocalisation Threshold plugin.

FRAP.

H3.1-/H4-EGFP wild type and mutants (FD, HB) were transfected into HEK293-F cells and seeded onto 8-well μ-slides (ibidi). FRAP experiments were performed using an UltraVIEW VoX Live Cell Imaging System (PerkinElmer) equipped with a PhotoKinesis FRAP module. Four pre-bleaching images of a single z-slice were taken before bleaching circular regions of 2 μm diameter in the cell nucleus using 30 iterations of the 405 nm laser at 50% power. Images were taken directly after bleaching, and every 15 seconds up to 4 min. Image analysis was performed in ImageJ. Values were normalised, taking the average of pre-bleach images as 1 and the lowest post-bleach image as 0. Error bars represent the s.d. of at least four individual experiments, containing each 2 to 5 bleached cells.

ACKNOWLEDGEMENTS

Facility support was provided by the Warwick Proteomics Research Technology Platform, CAMDU (Computing and Advanced Microscopy Development Unit), and Warwick Integrative Synthetic Biology (WISB) Centre (for access to flow cytometry facilities). We would like to acknowledge Andrew Bottrill, Cleidi Zampronio and Claire Mitchell for technical support, and colleagues in the Division of Biomedical Sciences at Warwick Medical School for support and advice. This work was supported by a Wellcome Trust Sir Henry Dale Fellowship to A. J. B. (208801/Z/17/Z).

References

1. C M Hammond, C B Stromme, H Huang, D J Patel, and A Groth. Histone chaperone networks shaping chromatin function. *Nat Rev Mol Cell Biol*, 2017.
2. Alonso J. Pardal, Filipe Fernandes-Duarte, and Andrew J. Bowman. The histone chaperoning pathway: from ribosome to nucleosome. *Essays in Biochemistry*, 63(1):29–43, March 2019.
3. R J Burgess and Z Zhang. Histone chaperones in nucleosome assembly and human disease. *Nat Struct Mol Biol*, 20(1):14–22, 2013. ISBN: 1545-9985 (Electronic) 1545-9985 (Linking).
4. D Filipescu, S Muller, and G Almouzni. Histone H3 variants and their chaperones during development and disease: contributing to epigenetic control. *Annu Rev Cell Dev Biol*, 30: 615–646, 2014. ISBN: 1530-8995 (Electronic) 1081-0706 (Linking).
5. Z A Gurard-Levin and G Almouzni. Histone modifications and a choice of variant: a language that helps the genome express itself. *F1000Prime Rep*, 6:76, 2014. ISBN: 2051-7599 (Linking).
6. Shweta Mendiratta, Alberto Gatto, and Genevieve Almouzni. Histone supply: Multitiered regulation ensures chromatin dynamics throughout the cell cycle. *The Journal of Cell Biology*, 218(1):39–54, January 2019.
7. Natalia Elisa Bernardes and Yuh Min Chook. Nuclear import of histones. *Biochemical Society Transactions*, 48(6):2753–2767, December 2020.
8. Yuh Min Chook and Katherine E. Süel. Nuclear import by karyopherin-betas: Recognition and inhibition. *Biochimica et Biophysica Acta (BBA) - Molecular Cell Research*, 1813(9): 1593–1606, September 2011.
9. M Baake, M Bauerle, D Doenecke, and W Albig. Core histones and linker histones are imported into the nucleus by different pathways. *Eur J Cell Biol*, 80(11):669–677, 2001.
10. P Muhlhausser, E C Muller, A Otto, and U Kutay. Multiple pathways contribute to nuclear import of core histones. *EMBO Rep*, 2(8):690–696, 2001.
11. N Mosammaparast, K R Jackson, Y Guo, C J Brame, J Shabanowitz, D F Hunt, and L F Pemberton. Nuclear import of histone H2A and H2B is mediated by a network of karyopherins. *Journal of Cell Biology*, 153(2):251–262, 2001.
12. N Mosammaparast, Y Guo, J Shabanowitz, D F Hunt, and L F Pemberton. Pathways mediating the nuclear import of histones H3 and H4 in yeast. *J Biol Chem*, 277(1):862–868, 2002.
13. J S Blackwell Jr., S T Wilkinson, N Mosammaparast, and L F Pemberton. Mutational analysis of H3 and H4 N termini reveals distinct roles in nuclear import. *J Biol Chem*, 282(28): 20142–20150, 2007.
14. Abhilash Padavannil, Prithwijit Sarkar, Seung Joong Kim, Tolga Cagatay, Jenny Jiou, Chad A Brautigam, Diana R Tomchick, Andrej Sali, Sheena D'Arcy, and Yuh Min Chook. Importin-9 wraps around the H2A-H2B core to act as nuclear importer and histone chaperone. *eLife*, 8:e43630, March 2019.
15. E I Campos and D Reinberg. New chaps in the histone chaperone arena. *Genes Dev*, 24 (13):1334–1338, 2010.
16. H Tagami, D Ray-Gallet, G Almouzni, and Y Nakatani. Histone H3.1 and H3.3 complexes mediate nucleosome assembly pathways dependent or independent of DNA synthesis. *Cell*, 116(1):51–61, 2004.
17. F Alvarez, F Munoz, P Schilcher, A Imhof, G Almouzni, and A Loyola. Sequential establishment of marks on soluble histones h3 and h4. *J Biol Chem*, 286(20):17714–17721, 2011.
18. M Soniat, T Cagatay, and Y M Chook. Recognition Elements in the Histone H3 and H4 Tails for Seven Different Importins. *J Biol Chem*, 291(40):21171–21183, 2016.
19. A Groth, D Ray-Gallet, J P Quivy, J Lukas, J Bartek, and G Almouzni. Human Asf1 regulates the flow of S phase histones during replicational stress. *Mol Cell*, 17(2):301–311, 2005.
20. M R Parthun, J Widom, and D E Gottschling. The major cytoplasmic histone acetyltransferase in yeast: links to chromatin replication and histone metabolism. *Cell*, 87(1):85–94, 1996. ISBN: 0092-8674 (Print) 0092-8674 (Linking).
21. Michael James Apta-Smith, Juan Ramon Hernandez-Fernaud, and Andrew James Bowman. Evidence for the nuclear import of histones H3.1 and H4 as monomers. *The EMBO journal*, 37(19):e98714, October 2018.
22. P L Paine, M E Johnson, Y T Lau, L J Tluczek, and D S Miller. The oocyte nucleus isolated in oil retains in vivo structure and functions. *Biotechniques*, 13(2):238–246, 1992. Edition: 1992/08/01 ISBN: 0736-6205 (Print) 0736-6205.
23. P L Paine, C F Austerberry, L J Desjarlais, and S B Horowitz. Protein loss during nuclear isolation. *J Cell Biol*, 97(4):1240–1242, 1983. Edition: 1983/10/01 ISBN: 0021-9525 (Print) 0021-9525.
24. M G O'Rand, R T Richardson, L J Zimmerman, and E E Widgren. Sequence and localization of human NASP: conservation of a Xenopus histone-binding protein. *Dev Biol*, 154(1):37–44, 1992.
25. O M Alekseev, E E Widgren, R T Richardson, and M G O'Rand. Association of NASP with HSP90 in mouse spermatogenic cells: stimulation of ATPase activity and transport of linker histones into nuclei. *J Biol Chem*, 280(4):2904–2911, 2005.
26. R T Richardson, I N Batova, E E Widgren, L X Zheng, M Whitfield, W F Marzluff, and M G O'Rand. Characterization of the histone H1-binding protein, NASP, as a cell cycle-regulated somatic protein. *J Biol Chem*, 275(39):30378–30386, 2000. Edition: 2000/07/14 ISBN: 0021-9258 (Print) 0021-9258 (Linking).
27. A J Cook, Z A Gurard-Levin, I Vassias, and G Almouzni. A specific function for the histone chaperone NASP to fine-tune a reservoir of soluble H3-H4 in the histone supply chain. *Mol Cell*, 44(6):918–927, 2011.
28. A Bowman, L Lercher, H R Singh, D Zinne, G Timinszky, T Carlomagno, and A G Ladurner. The histone chaperone sNASP binds a conserved peptide motif within the globular core of histone H3 through its TPR repeats. *Nucleic Acids Res*, 44(7):3105–3117, 2016.
29. Hongyu Bao, Massimo Carraro, Valentin Flury, Yanhong Liu, Min Luo, Liu Chen, Anja Groth, and Hongda Huang. NASP maintains histone H3–H4 homeostasis through two distinct H3 binding modes. *Nucleic Acids Research*, 50(9):5349–5368, May 2022.
30. Chao-Pei Liu, Wenxing Jin, Jie Hu, Mingzhu Wang, Jingjing Chen, Guohong Li, and Rui-Ming Xu. Distinct histone H3-H4 binding modes of sNASP reveal the basis for cooperation

DRAFT

and competition of histone chaperones. *Genes & Development*, 35(23-24):1610–1624, December 2021.

31. A Bowman, A Koide, J S Goodman, M E Colling, D Zinne, S Koide, and A G Ladurner. sNASP and ASF1A function through both competitive and compatible modes of histone binding. *Nucleic Acids Res*, 45(2):643–656, 2017.
32. Colin M. Hammond, Hongyu Bao, Ivo A. Hendriks, Massimo Carraro, Alberto García-Nieto, Yanhong Liu, Nazaret Reverón-Gómez, Christos Spanos, Liu Chen, Juri Rappsilber, Michael L. Nielsen, Dinshaw J. Patel, Hongda Huang, and Anja Groth. DNAJC9 integrates heat shock molecular chaperones into the histone chaperone network. *Molecular Cell*, 81 (12):2533–2548, April 2021.
33. S J Elsasser, H Huang, P W Lewis, J W Chin, C D Allis, and D J Patel. DAXX envelops an H3.3-H4 dimer for H3.3-specific recognition. *Nature*, 2012. Edition: 2012/10/19 ISBN: 1476-4687 (Electronic) 0028-0836 (Linking).
34. C M English, N K Maluf, B Tripet, M E A Churchill, and J K Tyler. ASF1 binds to a heterodimer of histones H3 and H4: A two-step mechanism for the assembly of the H3-H4 heterotetramer on DNA. *Biochemistry*, 44(42):13673–13682, 2005.
35. R Natsume, M Eitoku, Y Akai, N Sano, M Horikoshi, and T Senda. Structure and function of the histone chaperone CIA/ASF1 complexed with histones H3 and H4. *Nature*, 446(7133): 338–341, 2007.
36. H Huang, C B Stromme, G Saredi, M Hodl, A Strandsby, C Gonzalez-Aguilera, S Chen, A Groth, and D J Patel. A unique binding mode enables MCM2 to chaperone histones H3-H4 at replication forks. *Nat Struct Mol Biol*, 22(8):618–626, 2015. Edition: 2015/07/15 ISBN: 1545-9985.
37. N Richet, D Liu, P Legrand, C Velours, A Corpet, A Gaubert, M Bakail, G Moal-Raisin, R Guerois, C Compper, A Besle, B Guichard, G Almouzni, and F Ochsenbein. Structural insight into how the human helicase subunit MCM2 may act as a histone chaperone together with ASF1 at the replication fork. *Nucleic Acids Res*, 43(3):1905–1917, 2015. ISBN: 1362-4962 (Electronic) 0305-1048 (Linking).
38. Hong Wang, Mingzhu Wang, Na Yang, and Rui-Ming Xu. Structure of the quaternary complex of histone H3-H4 heterodimer with chaperone ASF1 and the replicative helicase subunit MCM2. *Protein & Cell*, 6(9):693–697, September 2015.
39. Ann K. Hogan, Kizhakke M. Sathyan, Alexander B. Willis, Sakshi Khurana, Shashank Srivastava, Ewelina Zasadzińska, Alexander S. Lee, Aaron O. Bailey, Matthew N. Gaynes, Jiehuan Huang, Justin Bodner, Celeste D. Rosencrance, Kelvin A. Wong, Marc A. Morgan, Kyle P. Eagen, Ali Shilatifard, and Daniel R. Foltz. UBR7 acts as a histone chaperone for post-nucleosomal histone H3. *The EMBO journal*, page e108307, November 2021.
40. Jianwei Lin, Xiucong Bao, and Xiang David Li. A tri-functional amino acid enables mapping of binding sites for posttranslational-modification-mediated protein-protein interactions. *Molecular Cell*, April 2021.
41. E I Campos, A H Smits, Y H Kang, S Landry, T M Escobar, S Nayak, B M Ueberheide, D Durocher, M Vermeulen, J Hurwitz, and D Reinberg. Analysis of the Histone H3.1 Interactome: A Suitable Chaperone for the Right Event. *Mol Cell*, 60(4):697–709, 2015.
42. Ralph E. Kleiner, Lisa E. Hang, Kelly R. Molloy, Brian T. Chait, and Tarun M. Kapoor. A Chemical Proteomics Approach to Reveal Direct Protein-Protein Interactions in Living Cells. *Cell Chemical Biology*, 25(1):110–120.e3, January 2018.
43. J P Lambert, M Tucholska, C Go, J D Knight, and A C Gingras. Proximity biotinylation and affinity purification are complementary approaches for the interactome mapping of chromatin-associated protein complexes. *J Proteomics*, 118:81–94, 2015.
44. Yosuke Isobe, Mikiko Okumura, Lynn M. McGregor, Scott M. Brittain, Michael D. Jones, Xiaoyou Liang, Ross White, William Forrester, Jeffrey M. McKenna, John A. Tallarico, Markus Schirle, Thomas J. Maimone, and Daniel K. Nomura. Manumycin polyketides act as molecular glues between UBR7 and P53. *Nature Chemical Biology*, 16(11):1189–1198, November 2020.
45. Eric D. Schwoebel, Thai H. Ho, and Mary Shannon Moore. The mechanism of inhibition of Ran-dependent nuclear transport by cellular ATP depletion. *The Journal of Cell Biology*, 157(6):963–974, June 2002.
46. K Zolghadr, O Mortusewicz, U Rothbauer, R Kleinhans, H Goehler, E E Wanker, M C Cardoso, and H Leonhardt. A fluorescent two-hybrid assay for direct visualization of protein interactions in living cells. *Mol Cell Proteomics*, 7(11):2279–2287, 2008. Edition: 2008/07/16 ISBN: 1535-9484 (Electronic) 1535-9476 (Linking).
47. S S Lam, J D Martell, K J Kamer, T J Deerinck, M H Ellisman, V K Mootha, and A Y Ting. Directed evolution of APEX2 for electron microscopy and proximity labeling. *Nat Methods*, 12(1):51–54, 2015.
48. Z Jasencakova, A N Scharf, K Ask, A Corpet, A Imhof, G Almouzni, and A Groth. Replication stress interferes with histone recycling and predeposition marking of new histones. *Mol Cell*, 37(5):736–743, 2010.
49. E I Campos, J Fillingham, G Li, H Zheng, P Voigt, W H Kuo, H Seepany, Z Gao, L A Day, J F Greenblatt, and D Reinberg. The program for processing newly synthesized histones H3.1 and H4. *Nat Struct Mol Biol*, 17(11):1343–1351, 2010.
50. K Ask, Z Jasencakova, P Menard, Y Feng, G Almouzni, and A Groth. Codanin-1, mutated in the anaemic disease CDAI, regulates Asf1 function in S-phase histone supply. *EMBO J*, 31(8):2013–2023, 2012.
51. Structure of Importin-4 bound to the H3-H4·ASF1 histone·histone chaperone complex, April 2022.
52. Steffen Frey, Renate Rees, Jürgen Schünemann, Sheung Chun Ng, Kevser Fünfgeld, Trevor Huyton, and Dirk Görlich. Surface Properties Determining Passage Rates of Proteins through Nuclear Pores. *Cell*, 174(1):202–217.e9, June 2018.
53. A Bowman, R Ward, N Wiechens, V Singh, H El-Mkami, D G Norman, and T Owen-Hughes. The histone chaperones Nap1 and Vps75 bind histones H3 and H4 in a tetrameric conformation. *Mol Cell*, 41(4):398–408, 2011. Edition: 2011/02/19 ISBN: 1097-4164 (Electronic) 1097-2765 (Linking).
54. D D Banks and L M Gloss. Folding mechanism of the (H3-H4)2 histone tetramer of the core nucleosome. *Protein Science*, 13(5):1304–1316, 2004.
55. Weidong Yang, Jeff Gelles, and Siegfried M. Musser. Imaging of single-molecule translocation through nuclear pore complexes. *Proceedings of the National Academy of Sciences of the United States of America*, 101(35):12887–12892, August 2004.
56. Ulrich Kubitscheck, David Grünwald, Andreas Hoekstra, Daniel Rohleder, Thorsten Kues, Jan Peter Siebrasse, and Reiner Peters. Nuclear transport of single molecules: dwell times at the nuclear pore complex. *The Journal of Cell Biology*, 168(2):233–243, January 2005.
57. U. Jakob, M. Gaestel, K. Engel, and J. Buchner. Small heat shock proteins are molecular chaperones. *The Journal of Biological Chemistry*, 268(3):1517–1520, January 1993.
58. Evgeny V. Mymrikov, Marina Daake, Bettina Richter, Martin Haslbeck, and Johannes Buchner. The Chaperone Activity and Substrate Spectrum of Human Small Heat Shock Proteins. *The Journal of Biological Chemistry*, 292(2):672–684, January 2017.
59. Heath Ecroyd. Redefining the Chaperone Mechanism of sHsps: Not Just Holdase Chaperones. In Robert M. Tanguay and Lawrence E. Hightower, editors, *The Big Book on Small Heat Shock Proteins*, Heat Shock Proteins, pages 179–195. Springer International Publishing, Cham, 2015.
60. Mikko Taipale, George Tucker, Jian Peng, Irina Krykbaeva, Zhen-Yuan Lin, Brett Larsen, Hyungwon Choi, Bonnie Berger, Anne-Claude Gingras, and Susan Lindquist. A quantitative chaperone interaction network reveals the architecture of cellular protein homeostasis pathways. *Cell*, 158(2):434–448, July 2014.
61. Axel Mogk and Bernd Bukau. Role of sHsps in organizing cytosolic protein aggregation and disaggregation. *Cell Stress & Chaperones*, 22(4):493–502, July 2017.
62. Kevin Reinle, Axel Mogk, and Bernd Bukau. The Diverse Functions of Small Heat Shock Proteins in the Proteostasis Network. *Journal of Molecular Biology*, page 167157, July 2021.
63. Juan Hormazabal, Francisco Saavedra, Claudia Espinoza-Arratia, Nicolas W Martinez, Tatiana Cruces, Iván E Alfaro, and Alejandra Loyola. Chaperone mediated autophagy contributes to the newly synthesized histones H3 and H4 quality control. *Nucleic Acids Research*, 50(4):1875–1887, February 2022.
64. Y Li, L Zhang, T Liu, C Chai, Q Fang, H Wu, P A Agudelo Garcia, Z Han, S Zong, Y Yu, X Zhang, M R Parthun, J Chai, R M Xu, and M Yang. Hat2p recognizes the histone H3 tail to specify the acetylation of the newly synthesized H3/H4 heterodimer by the Hat1p/Hat2p complex. *Genes Dev*, 28(11):1217–1227, 2014.
65. A Verreault, P D Kaufman, R Kobayashi, and B Stillman. Nucleosomal DNA regulates the core-histone-binding subunit of the human Hat1 acetyltransferase. *Curr Biol*, 8(2):96–108, 1998.
66. Ye Yue, Wen-Si Yang, Lin Zhang, Chao-Pei Liu, and Rui-Ming Xu. Topography of histone H3–H4 interaction with the Hat1–Hat2 acetyltransferase complex. *Genes & Development*, April 2022. Company: Cold Spring Harbor Laboratory Press Distributor: Cold Spring Harbor Laboratory Press Institution: Cold Spring Harbor Laboratory Press Label: Cold Spring Harbor Laboratory Press Publisher: Cold Spring Harbor Lab.
67. D R Foltz, L E Jansen, A O Bailey, J R Yates 3rd, E A Bassett, S Wood, B E Black, and D W Cleveland. Centromere-specific assembly of CENP-a nucleosomes is mediated by HJURP. *Cell*, 137(3):472–484, 2009.
68. Santanu Adhikary, Deepavali Chakravarti, Christopher Terranova, Isha Sengupta, Mayinuer Maitituoheti, Anirban Dasgupta, Dushyant Kumar Srivastava, Junsheng Ma, Ayush T. Raman, Emily Tarco, Aysegul A. Sahin, Roland Bassett, Fei Yang, Coya Tapia, Siddhartha Roy, Kunal Rai, and Chandrima Das. Atypical plant homeodomain of UBR7 functions as an H2BK120Ub ligase and breast tumor suppressor. *Nature Communications*, 10(1):1398, March 2019.
69. D G Gibson. Synthesis of DNA fragments in yeast by one-step assembly of overlapping oligonucleotides. *Nucleic Acids Res*, 37(20):6984–6990, 2009.
70. F. Ann Ran, Patrick D. Hsu, Jason Wright, Vineeta Agarwala, David A. Scott, and Feng Zhang. Genome engineering using the CRISPR-Cas9 system. *Nature Protocols*, 8(11): 2281–2308, November 2013.
71. Abhilash Padavannil, Chad A. Brautigam, and Yuh Min Chook. Molecular Size Analysis of Recombinant Importin-histone Complexes Using Analytical Ultracentrifugation. *Bio-Protocol*, 10(10):e3625, May 2020.
72. K Luger, T J Rechsteiner, A J Flaus, M M Waye, and T J Richmond. Characterization of nucleosome core particles containing histone proteins made in bacteria. *J Mol Biol*, 272(3): 301–311, 1997. ISBN: 0022-2836 (Print) 0022-2836 (Linking).
73. Sarah E. McClelland and Andrew D. McAinsh. Hydrodynamic Analysis of Human Kinetochore Complexes During Mitosis. In Andrew D. McAinsh, editor, *Mitosis: Methods and Protocols*, Methods in Molecular Biology, pages 81–98. Humana Press, Totowa, NJ, 2009.
74. K Suzuki, P Bose, R Y Leong-Quong, D J Fujita, and K Riabowol. REAP: A two minute cell fractionation method. *BMC Res Notes*, 3:294, 2010.
75. Andrej Shevchenko, Henrik Tomas, Jan Havli, Jesper V. Olsen, and Matthias Mann. In-gel digestion for mass spectrometric characterization of proteins and proteomes. *Nature Protocols*, 1(6):2856–2860, December 2006.
76. Stefka Tyanova, Tikira Temu, and Juergen Cox. The MaxQuant computational platform for mass spectrometry-based shotgun proteomics. *Nature Protocols*, 11(12):2301–2319, December 2016.
77. Matthew E. Ritchie, Belinda Phipson, Di Wu, Yifang Hu, Charity W. Law, Wei Shi, and Gordon K. Smyth. limma powers differential expression analyses for RNA-sequencing and microarray studies. *Nucleic Acids Research*, 43(7):e47, April 2015.
78. Yasset Perez-Riverol, Attila Csordas, Jingwen Bai, Manuel Bernal-Llinares, Suresh Hewapathirana, Deepti J Kundu, Avinash Inuganti, Johannes Griss, Gerhard Mayer, Martin Eisenacher, Enrique Pérez, Julian Uszkoreit, Julianus Pfeuffer, Timo Sachsenberg, Şule Yılmaz, Shivani Tiwary, Jürgen Cox, Enrique Audain, Mathias Walzer, Andrew F Jarnuczak, Tobias Ternent, Alvis Brazma, and Juan Antonio Vizcaíno. The PRIDE database and related tools and resources in 2019: improving support for quantification data. *Nucleic Acids Research*, 47(D1):D442–D450, January 2019.

DRAFT

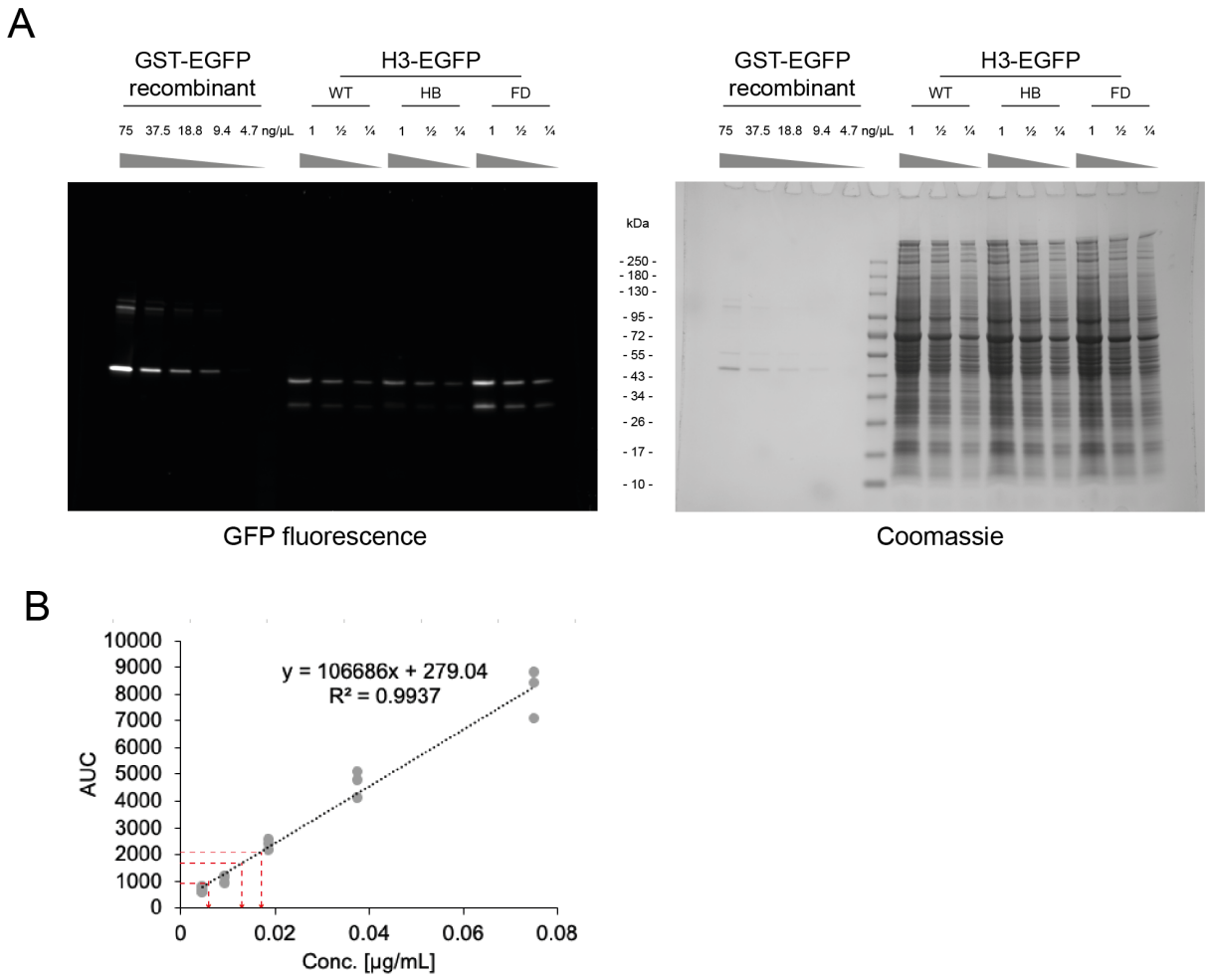

Figure S1. Related to Fig 2. Calibration for precise input quantification.
A: Residual fluorescence activity of GFP constructs on a semi-denaturing gel before staining (left) and after Coomassie staining (right). B: Area under the curve (AUC) analysis of residual GFP fluorescent bands, for GST-GFP calibration curve and sample dilutions (red line).

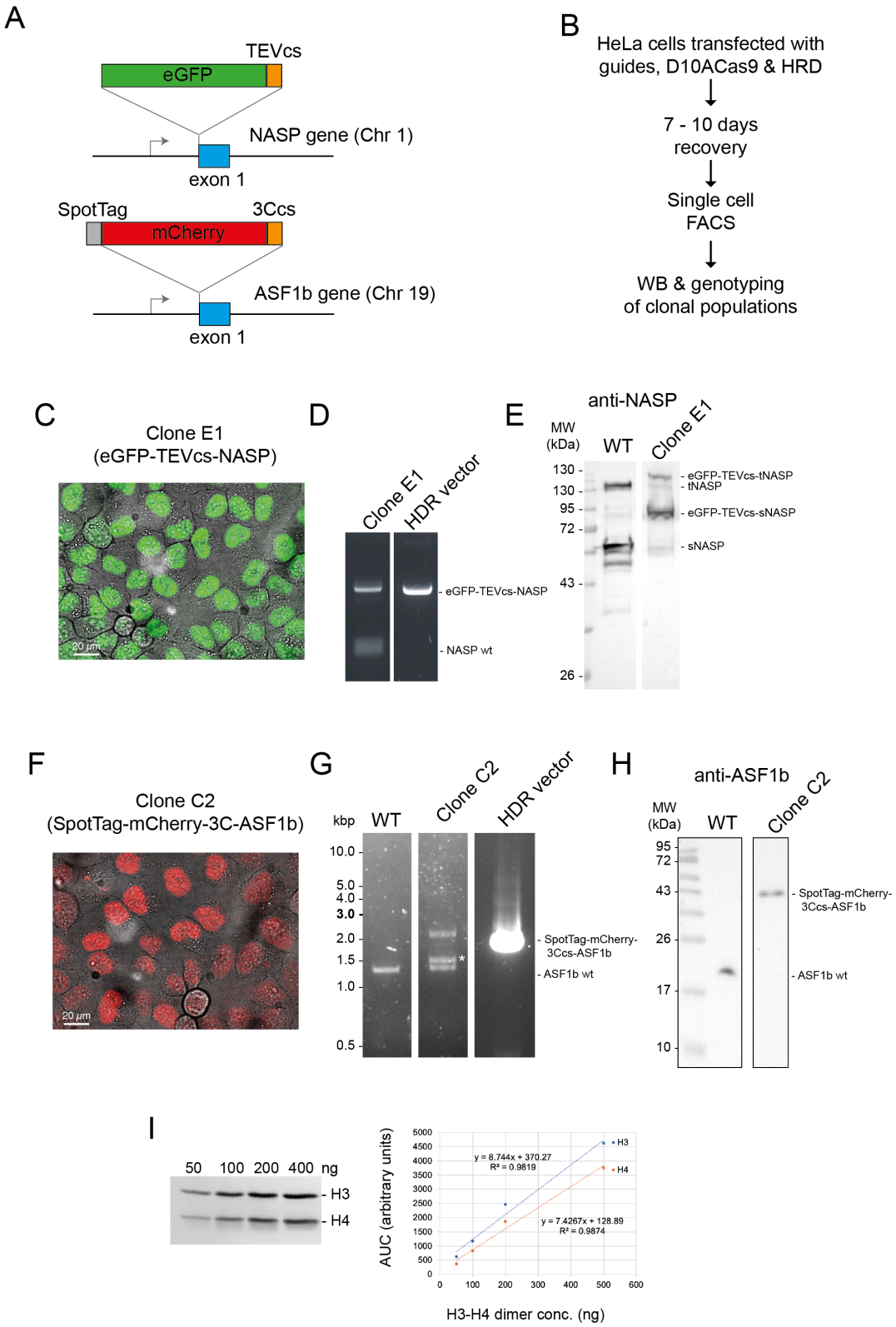

Figure S2. Related to Fig 3.
A: Experimental design for CRISPR Knock-in cell line selection, western blot (WB) and PCR validation of the clonal lines. B: Confocal microscopy for selected CRISPR Knock-in cell lines EGFP-NASP and mCherry- ASF1B, demonstrate nuclear localisation, even expression and complete penetration. C: Serial dilutions for H3-H4 quantification. 50–400 ng of H3-H4 dimer was separated by SDS–PAGE and stained with Coomassie as previously described (Apta-smith et al., 2018).

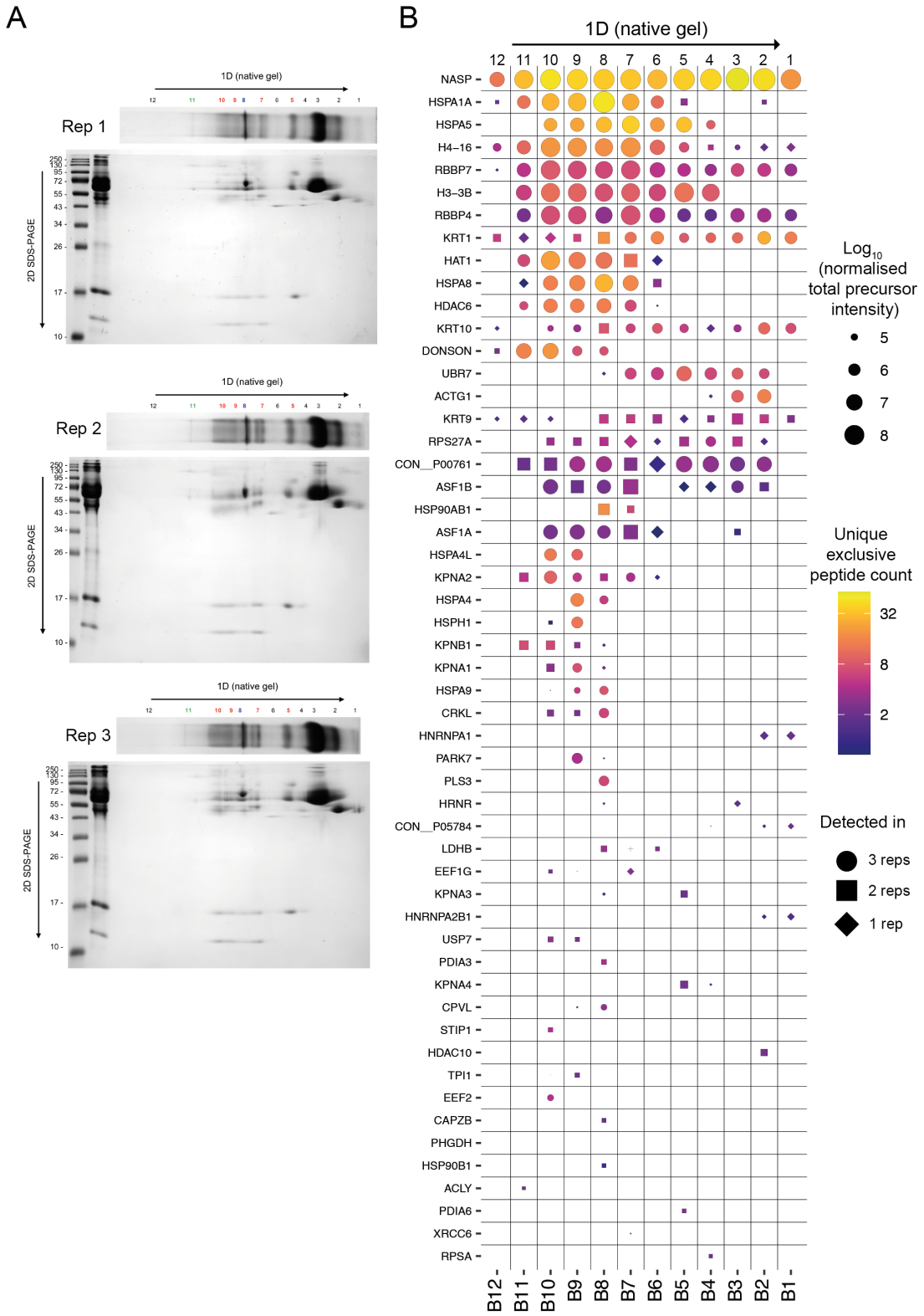

Figure S3. Related to Fig 3.
A: Native gel (1D) and SDS-PAGE (2D) for 3 independent experiments (performed with different batches of cell transfected on different days, processed subsequently 36 hrs after transfection). B: Mass-spectrometry identification of NASP-interacting factors from native gel bands (cut as labelled in A).

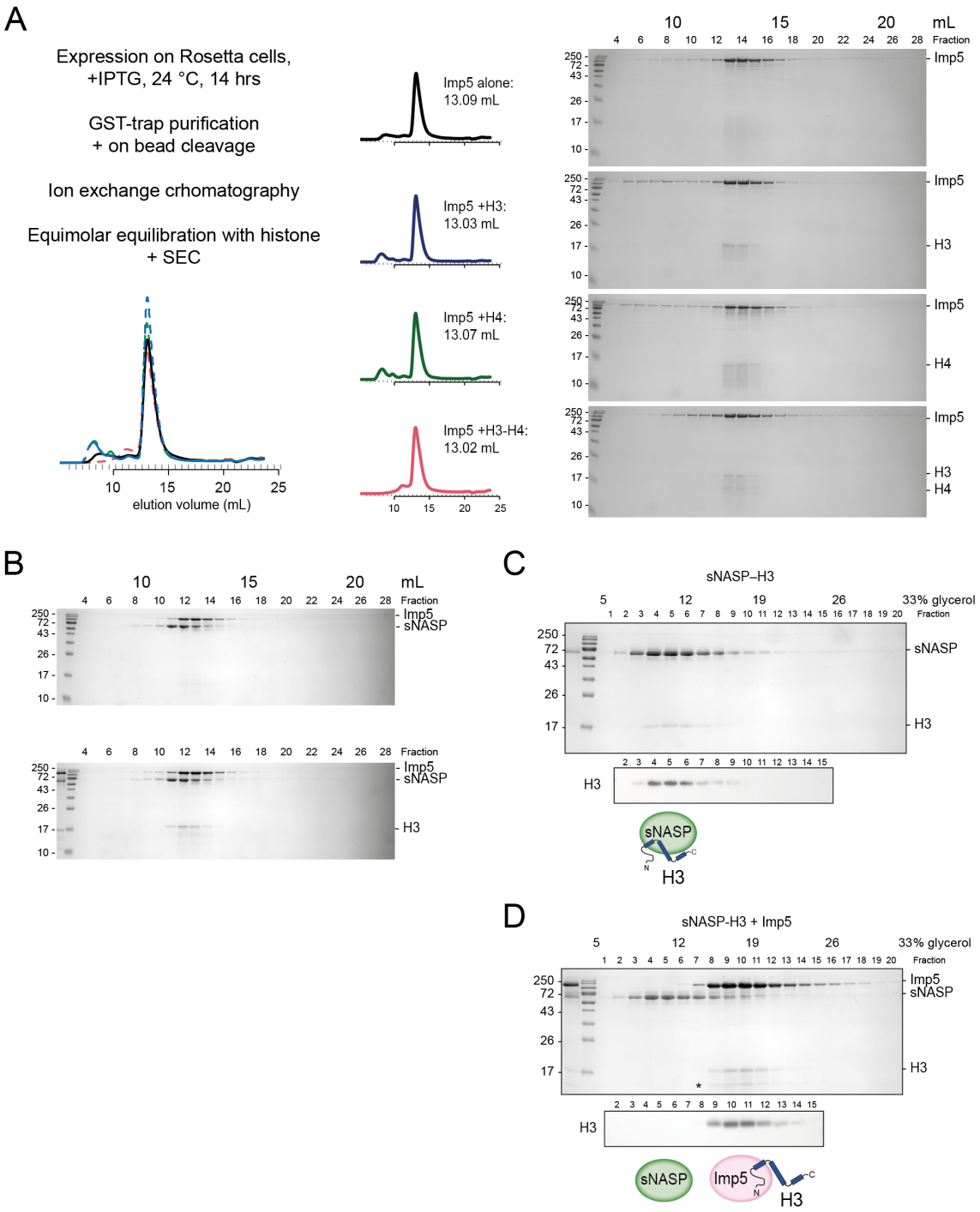

Figure S4. Related to Fig 4.
A: Experimental design for Imp5 purification and complex reconstitution, SEC_{280} trace (on Superdex Increase 200), peak volumes (mL) and Coomassie-stained gels. B: SEC for sNASP + Imp5 does not resolve these proteins (i.e. elution peaks at ~12.6 and 13 mL respectively). C: 5-40\% glycerol gradient ultracentrifugation (240,000 g, 4 °C, 12 hours) sNASP-H3. D: Imp5 outcompetes pre-formed sNASP-H3 and displaces H3. (equimolar mix).

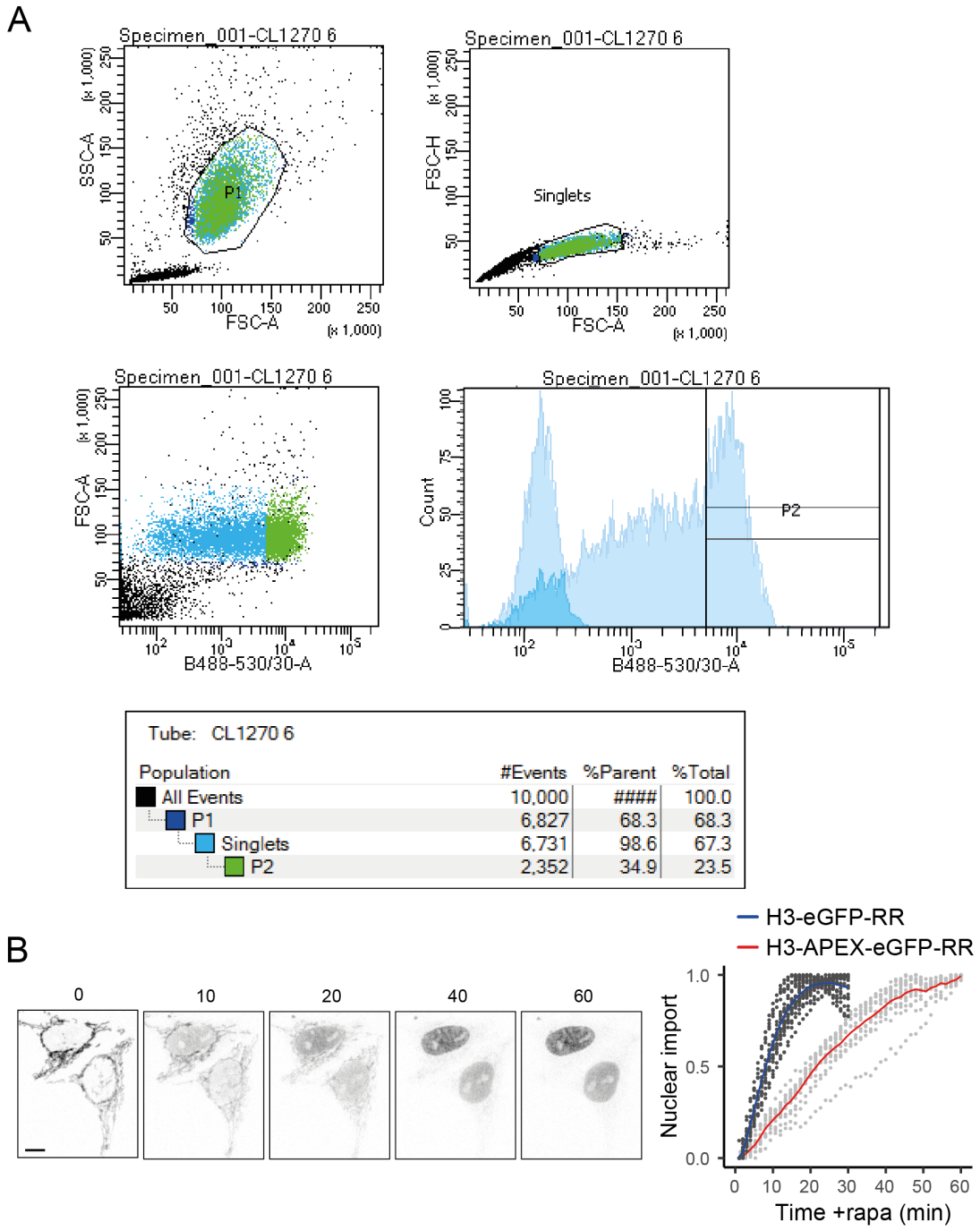

Figure S5. Related to Fig 5. A
A: FACS data for FRT -H3-APEX2-EGFP-RR cells induced with doxycycline for 12 hours, compared to non-induced cells (faded) in blue laser histogram (bottom right graph). B: Confocal microscopy time course of doxycycline-induced FRT-H3-APEX2-EGFP-RR and nuclear enrichment analysis (red) compared to H3-eGFP-RAPID release (RR) in blue. Note that the addition of the APEX2 tag delays the cleavage kinetics and nuclear localisation.

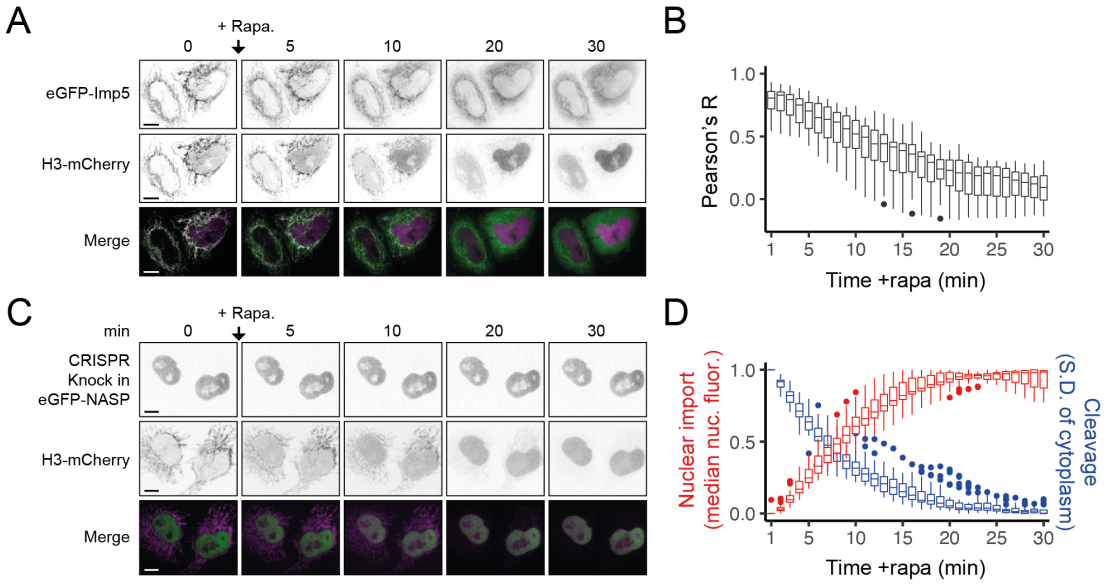

Figure S6. Related to Fig 6.
A: Confocal microscopy time course after the addition of rapamycin (RAPID release H3-mCherry-RR) in cells transiently expressing eGFP-Imp5. Bar = 10 µm. B: Pearson's correlation coefficient (R) analysis (as in A. n = 20 cells). C: Confocal microscopy time course after the addition of rapamycin (RAPID release H3-eGFP-RR) in HeLa cells with eGFP-NASP endogenously labelled (CRISPR knock-in). Bar = 10 µm. D nuclear enrichment analysis compared to cleavage rate (inferred from S.D of cytoplasm).

Fig 1E

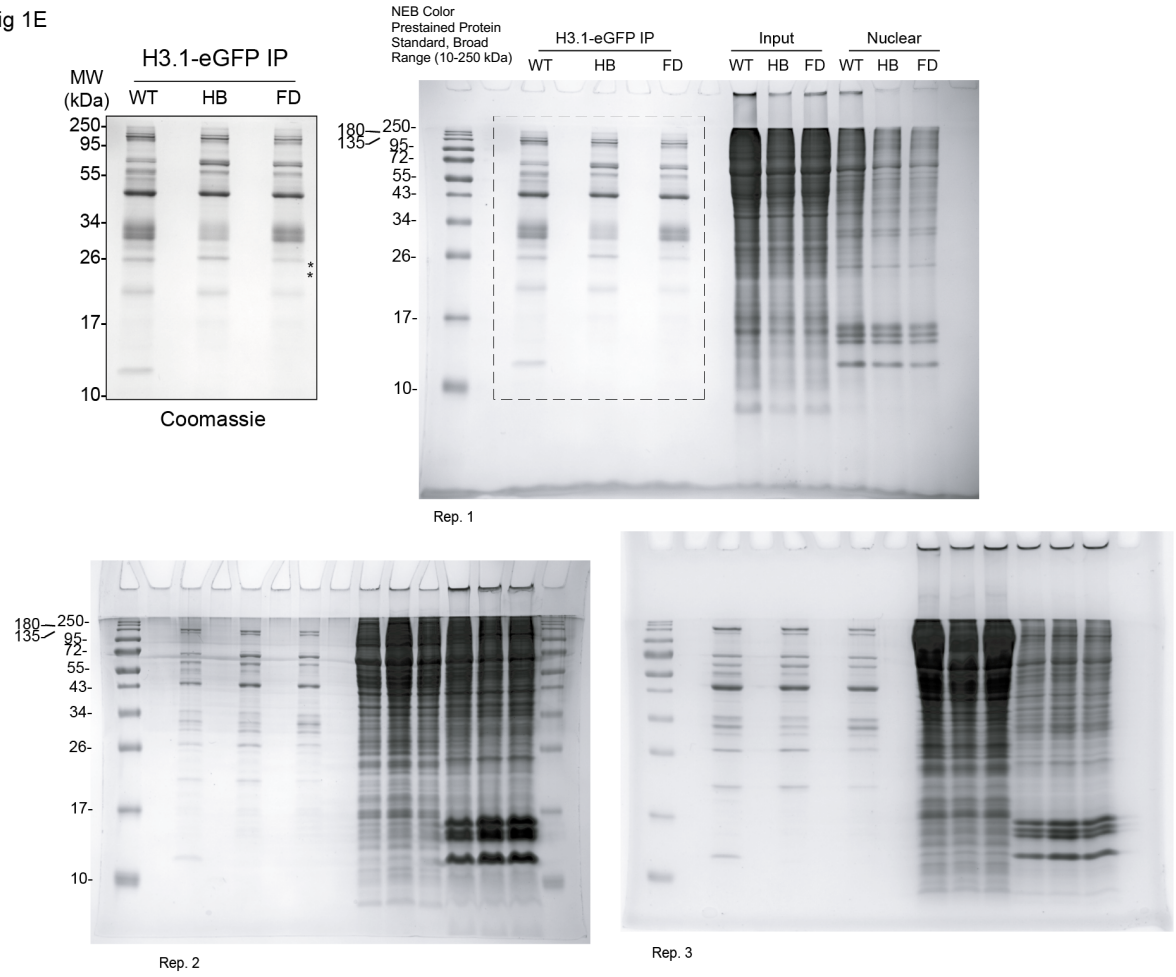
H3.1-eGFP IP
MW (kDa)
WT HB FD
250- 95- 55- 34- 26- 17- 10-
Coomassie
NEB Color Prestained Protein Standard, Broad Range (10-250 kDa)
H3.1-eGFP IP
Input
Nuclear
WT HB FD WT HB FD WT HB FD
180 135 250- 95- 72- 55- 43- 34- 26- 17- 10-
Rep. 1
Rep. 2
Rep. 3

Fig 1F

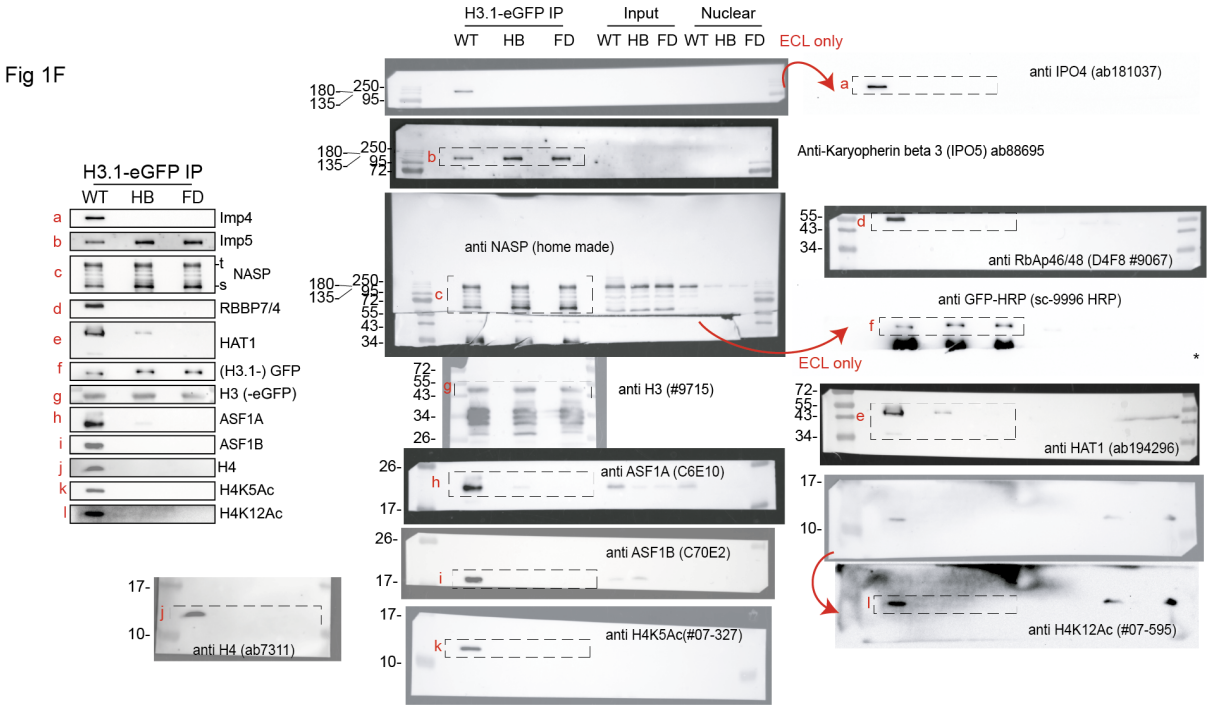
H3.1-eGFP IP
WT HB FD
a Imp4
b Imp5
c NASP t s
d RBBP7/4
e HAT1
f (H3.1-) GFP
g H3 (-eGFP)
h ASF1A
i ASF1B
j H4
k H4K5Ac
l H4K12Ac
H3.1-eGFP IP
Input
Nuclear
WT HB FD WT HB FD WT HB FD
ECL only
anti IPO4 (ab181037)
Anti-Karyopherin beta 3 (IPO5) ab88695
anti NASP (home made)
anti RbAp46/48 (D4F8 #9067)
anti GFP-HRP (sc-9996 HRP)
ECL only
anti H3 (#9715)
anti HAT1 (ab194296)
anti ASF1A (C6E10)
anti ASF1B (C70E2)
anti H4K5Ac(#07-327)
anti H4 (ab7311)
anti H4K12Ac (#07-595)

Fig 1E

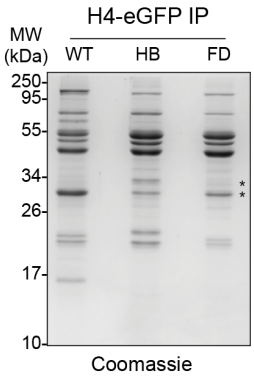

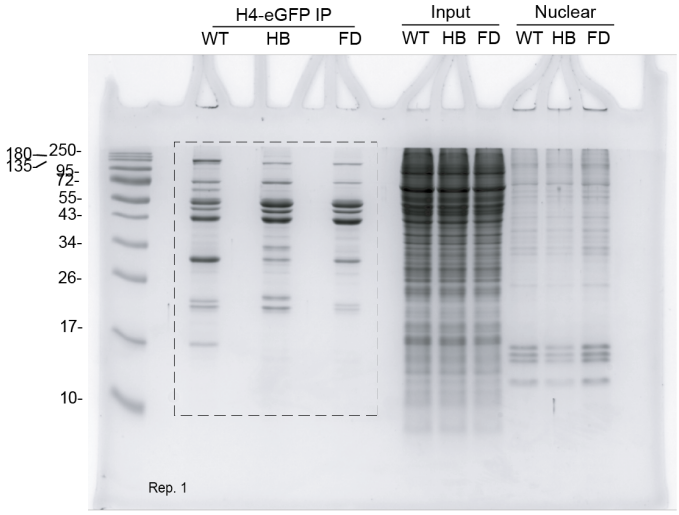

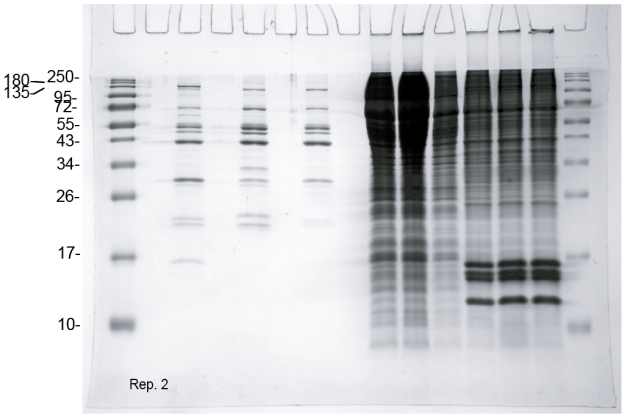

Rep. 3 Coomassie staining unavailable

Fig 1F

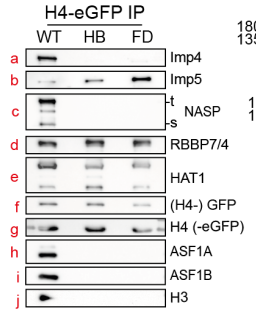

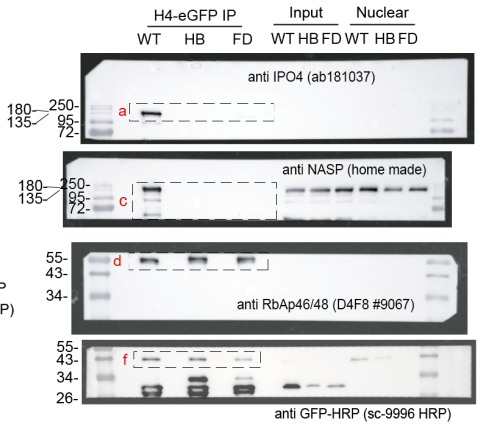

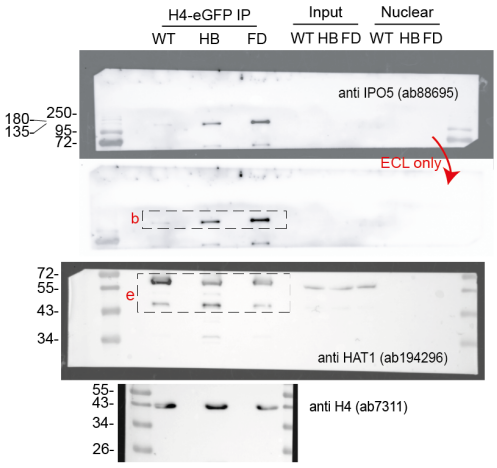

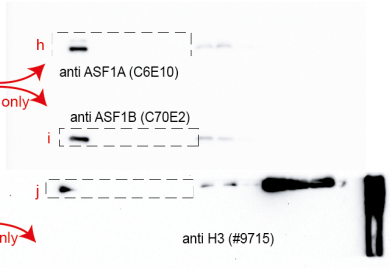

Fig 3B

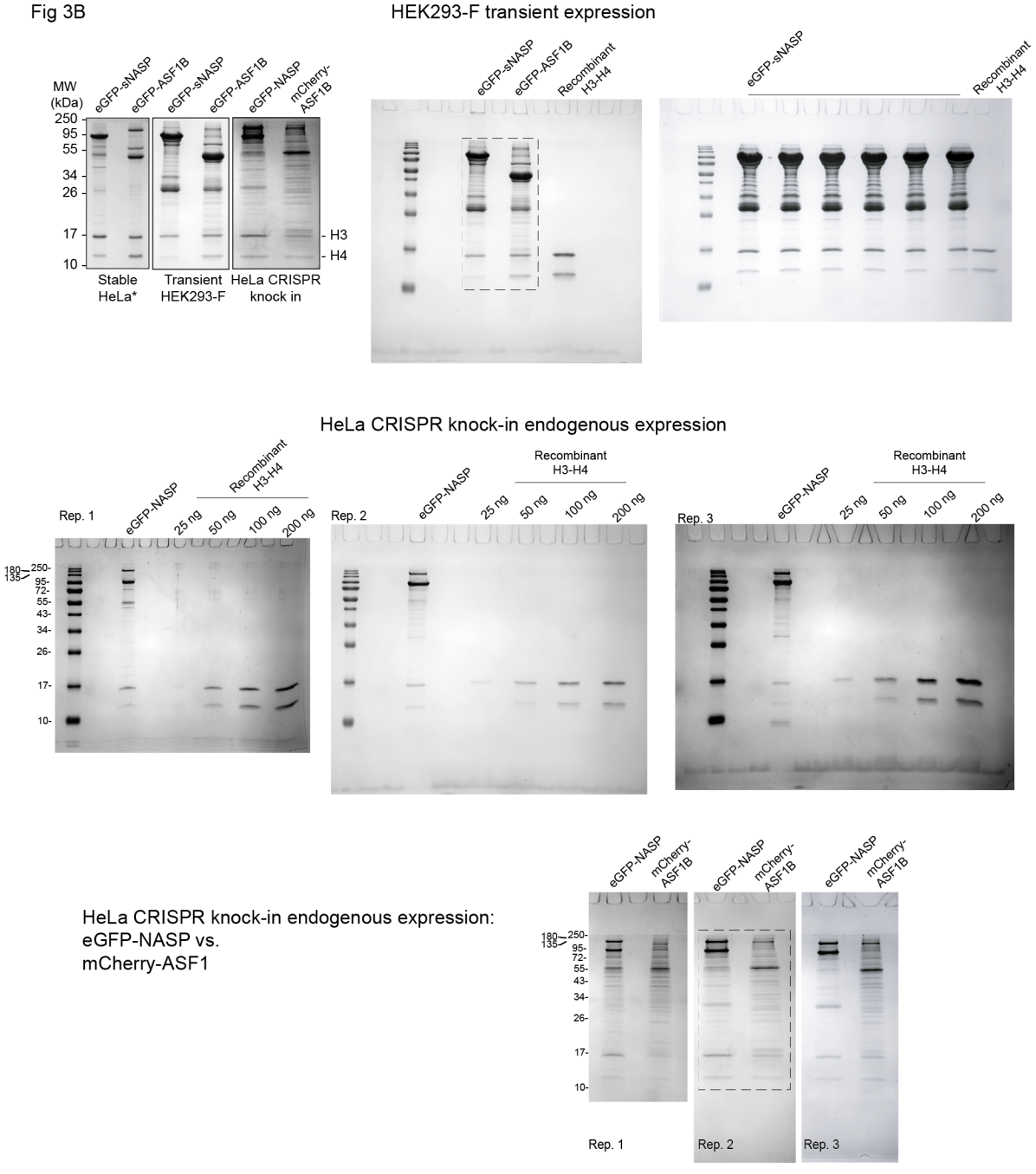
HEK293-F transient expression
MW (kDa)
eGFP-sNASP
eGFP-ASF1B
eGFP-sNASP
eGFP-ASF1B
eGFP-NASP
mCherry-ASF1B
250
95
55
34
26
17
10
H3
H4
Stable HeLa*
Transient HEK293-F
HeLa CRISPR knock in
eGFP-sNASP
eGFP-ASF1B
Recombinant H3-H4
eGFP-sNASP
Recombinant H3-H4
HeLa CRISPR knock-in endogenous expression
Rep. 1
eGFP-NASP
Recombinant H3-H4
25 ng
50 ng
100 ng
200 ng
180
135
250-
95-
72-
55-
43-
34-
26-
17-
10-
Rep. 2
eGFP-NASP
Recombinant H3-H4
25 ng
50 ng
100 ng
200 ng
Rep. 3
eGFP-NASP
Recombinant H3-H4
25 ng
50 ng
100 ng
200 ng
HeLa CRISPR knock-in endogenous expression:
eGFP-NASP vs.
mCherry-ASF1
eGFP-NASP
mCherry-ASF1B
eGFP-NASP
mCherry-ASF1B
eGFP-NASP
mCherry-ASF1B
180
135
250-
95-
72-
55-
43-
34-
26-
17-
10-
Rep. 1
Rep. 2
Rep. 3

Fig 3D

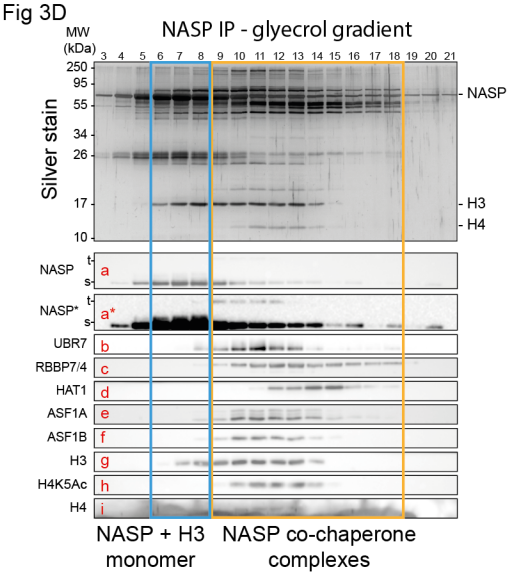

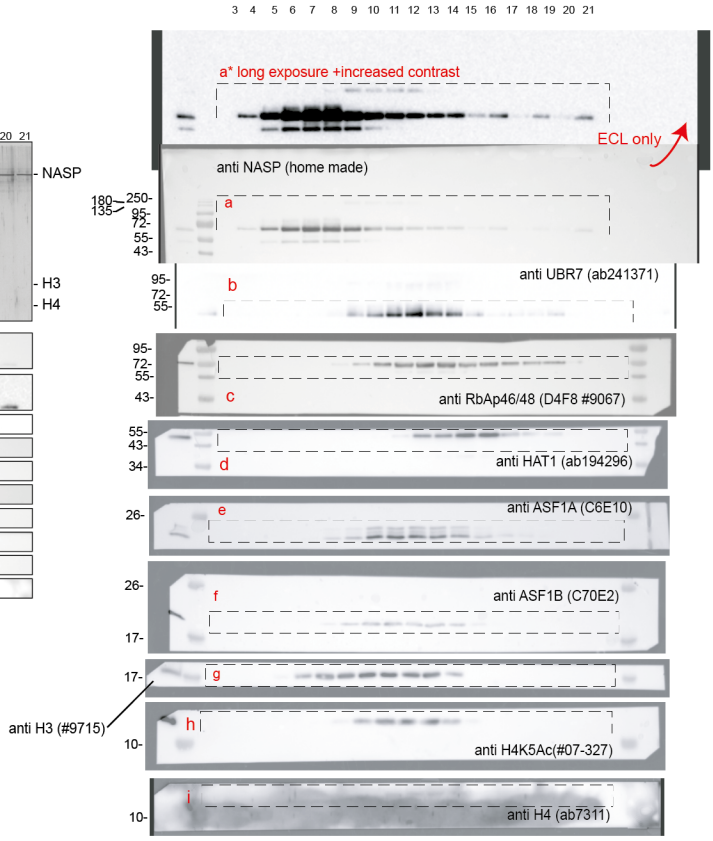

For replicates of the stained native gels (send for mass spectrometry) and 2D gels see Supp. Fig. 3

Fig 3E

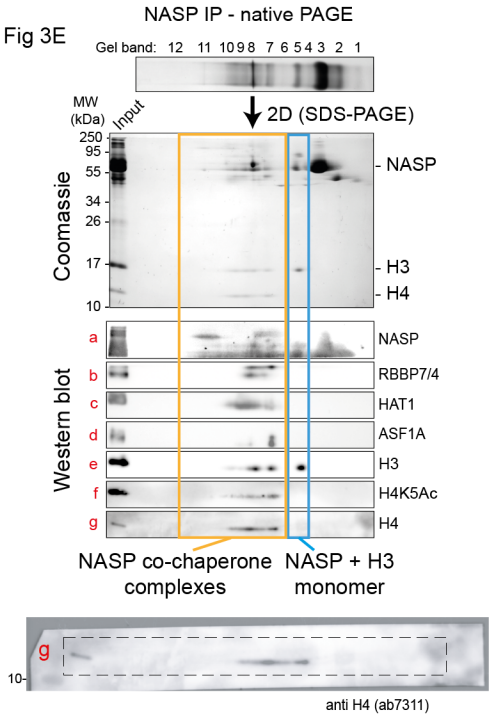

To avoid excessive background, anti NASP primary antibody was incubated with anti Rabbit alexa 561 conguated (unlike the remaining blots in this work, where the secondary antibody was HRP congugated)

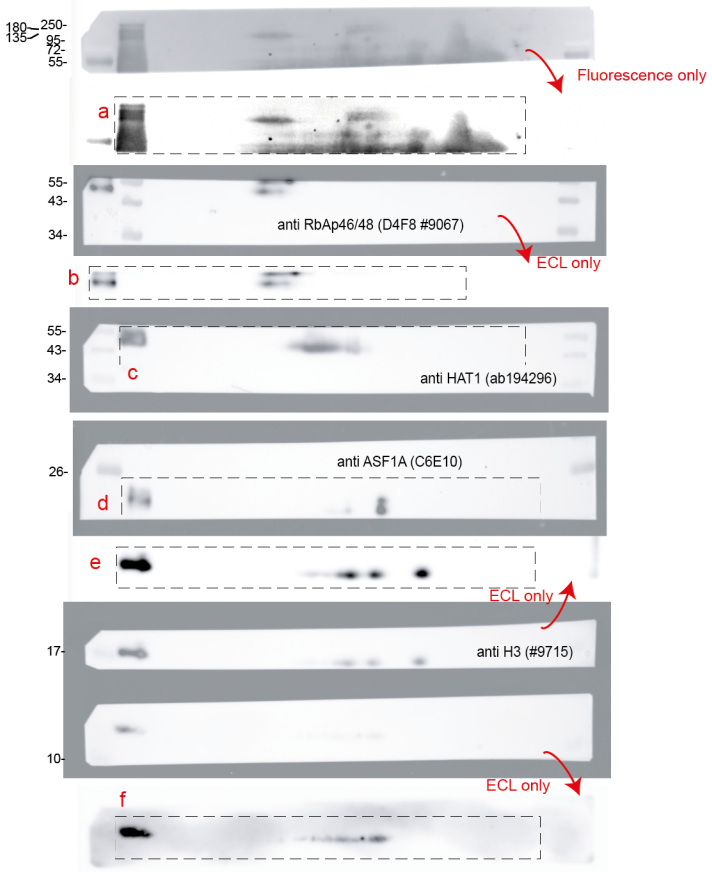

Fig 4A

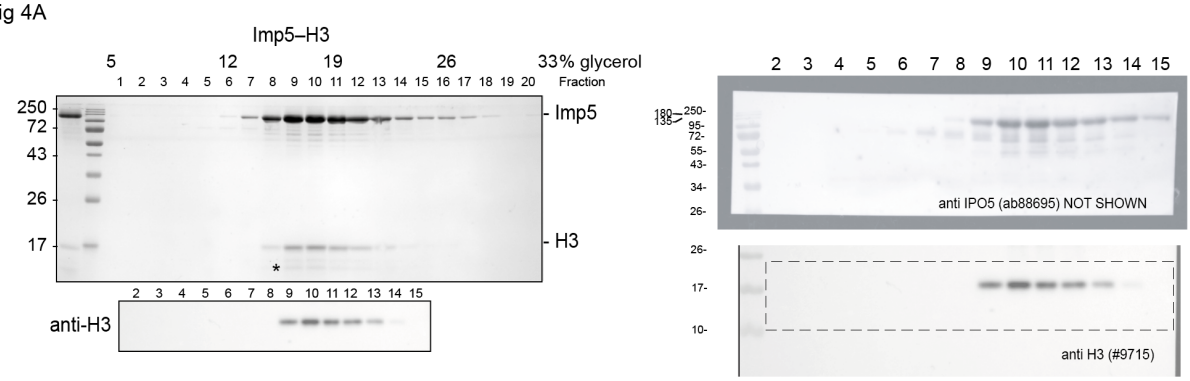

Fig 4B

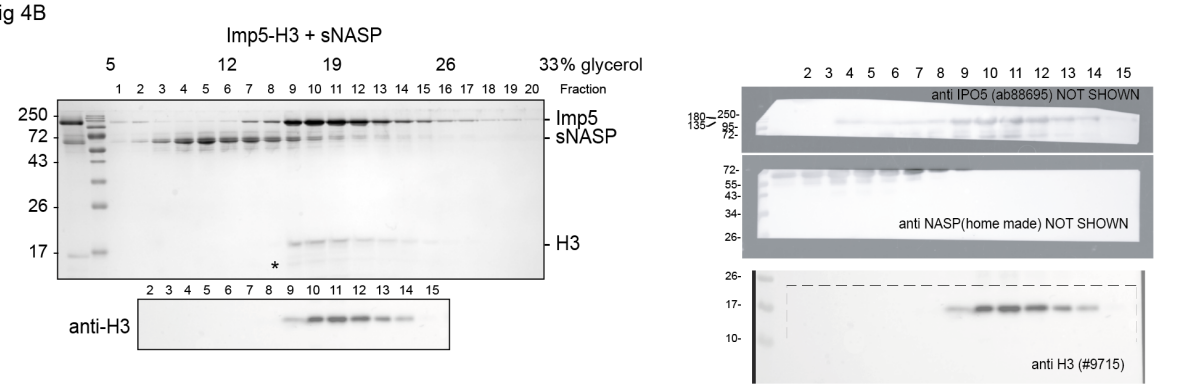

Fig 4C

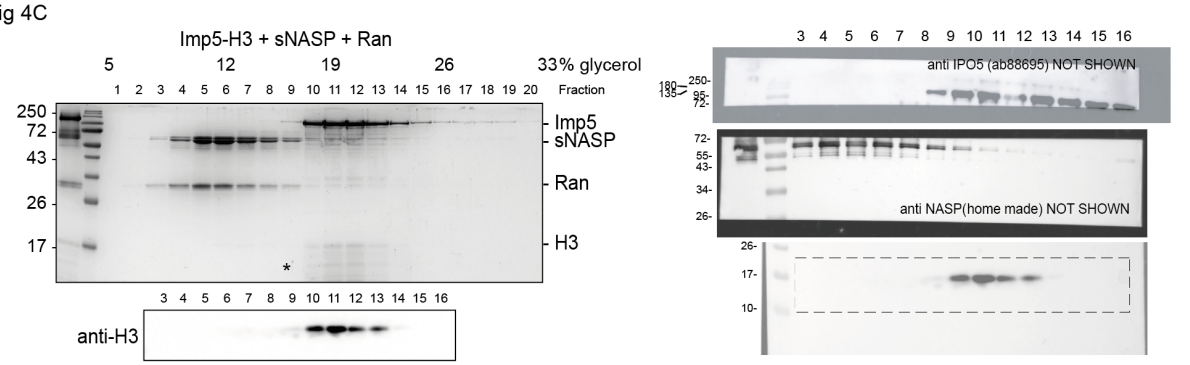

Fig 4D

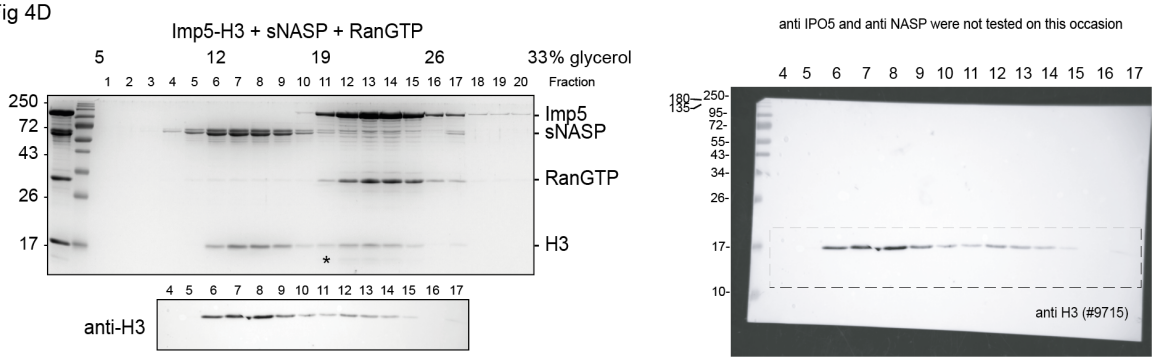

Fig 6 B

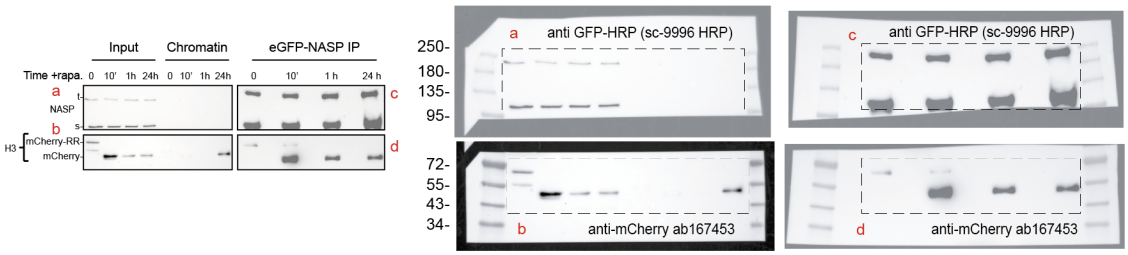

Rep. 2

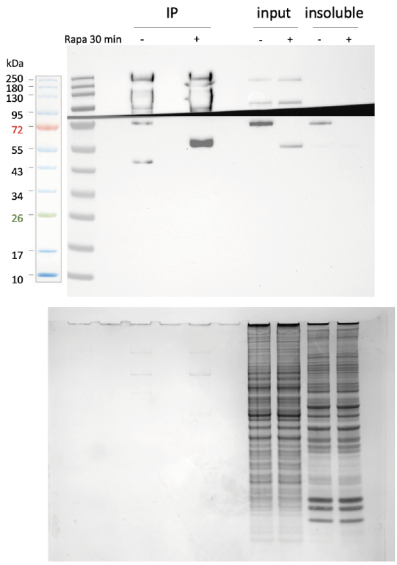

Rep. 3

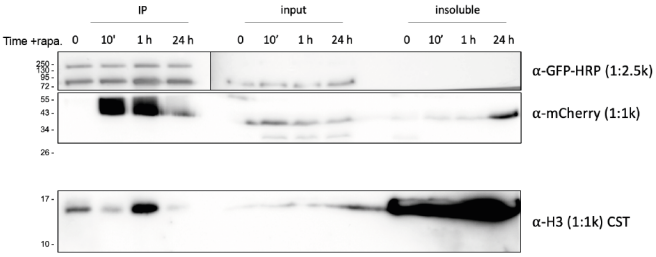

Table S1. Plasmids used in this study.

Plasmid name	Construct	Backbone	Origin
H3-GFP	H3.1-EGFP	pEGFP-N1	Apta-Smith et al., 2018.
H3 HB-GFP	H3.1 (A95_GGG)-EGFP	pEGFP-N1	This study
H3 FD-GFP	H3.1 (FLY>AAA)-EGFP	pEGFP-N1	This study
H4-GFP	H4-EGFP	pEGFP-N1	Apta-Smith et al., 2018.
H4 HB-GFP	H4 (V65GGG)-EGFP	pEGFP-N1	This study
H4 FD-GFP	H4 (FLI>AAA)-EGFP	pEGFP-N1	This study
H3-mCherry-RR	H3.2-mCherry-2xTVMVcs-FRB-OMP5–IRES–FKBP-TVMV-AI	pEGFP-C1	This study
GFP-Imp5	EGFP-Imp5	pEGFP-C1	This study
GFP-sNASP	EGFP-TEV-sNASP	pIRESpuro2	This study
H3-APEX2-EGFP-RR	H3.1-Flag-APEX2-EGFP-2xTVMVcs-FRB-OMP25-IRES-FKBP-TVMV-AI	pcDNA™5/FRT/TO	This study
NASP_HDR	pNASP-EGFP-TEV_HDR-donor	pBlueScript II KS (+)	This study
NASP_sgRNA_Down	pX461-NASP-sgRNA2-down	pX461-PSPCas9N(BB)-2A-GFP	This study
NASP_sgRNA_up	pX461-NASP-sgRNA2-up	pX461-PSPCas9N(BB)-2A-GFP	This study
ASF1B_HDR	pASF1b-Spot-mCherry-3C_HDR-donor	pBlueScript II KS (+)	This study
ASF1B_sgRNA_Down	pX461-ASF1B-sgRNA2-down	pX461-PSPCas9N(BB)-2A-GFP	This study
ASF1B_sgRNA_up	pX461-ASF1B-sgRNA2-up	pX461-PSPCas9N(BB)-2A-GFP	This study
GST-Imp5	pGST-HRV 3Ccs-Imp5 iso1	pGEX-6P1	This study

Table S2. Primers and gene fragments sequences

Primer_name	Sequence
XhoI_IPO5_F	aaaaaaCTCGAGcaATGGCGGCGGCCGC
KpnI_IPO5_R	GGTGGTggtaccTCACGCAGAGTTCAGGAGCTC
IPO5_pGEX_F	ctgttccaggggcccctgggatccGCAATGGCGGCGGCtGCG
IPO5_pGEX_R	gtcagtcagtcacgatgcggccgcTCACGCAGAGTTCAGGAGC
Kozak5p_F	TGAACCGTCAGATCCGCTAGC
OMP25_IRES_R	CGGTAGCGCTACAGCTGTTTGCGATAGCG
OMP25_IRES_F	TCGCAAACAGCTGTAGCGCTACCGGACTCAG
IRES_FKBP_R	TCCACCTGCACCATGGTTGTGGCCATAT
FKBP_IRES_F	ATGGCCACAACCATGGTGCAGGTGGAAACC
FKBP_FRT_R	TGTGGGAGGTTTCTAGCTGCCCGGCGC
FRT_AI_F	CCGGGCAGCTAGAAACCTCCCACACCTCCCCCT
Kozak_H3.1_R	GATCTGACGGTTCACTAAAC
APEX2_gBLOCK	AGCGCTACCGGTCGCCACCATGGACTACAAGGATGACGACGATAAGGGAAAGTCTTACCCAACTGTGAGTGCTGATTACCAGGACGCCGTTGAGAAGGCGAAGAAGAAGCTC AGAGGCTTCATCGCTGAGAAGAGATGCGCTCCTCTAATGCTCCGTTTGGCATTCCACTCTGCTGGAACCTTTGACAAGGGCACGAAGACCGGaGGACCCTTCGGAACCATCAA GCACCCTGCCGAACTGGCTCACAGCGCTAACAACGGTCTTGACATCGCTGTTAGGCTTTTGGAGCCACTCAAGGCGGAGTTCCCTATTTTGAGCTACGCCGATTTCTACCAGTT GGCTGGCGTTGTTGCCGTTGAGGTCACGGGTGGACCTAAGGTTCCATTCCACCCTGGAAGAGAGGACAAGCCTGAGCCACCACCAGAGGGTCGCTTGCCCGATCCCACTAAG GGTTCTGACCATTTGAGAGATGTGTTTGGCAAAGCTATGGGGCTTACTGACCAAGATATCGTTGCTCTATCTGGGGGTCACACTATTGGAGCTGCACACAAGGAGCGTTCTGGA TTTGAGGGTCCCTGGACCTCTAATCCTCTTATTTTCGACAACTCATACTTCACGGAGTTGTTGAGTGGTGAGAAGGAAGGaCTCCTTCAGCTACCTTCTGACAAGGCTCTTTTGT CTGACCCTGTATTCCGCCCTCTCGTTGACAAATATGCAGCGGACGAAGATGCCTTCTTTGCTGATTACGCTGAGGCTCACCAAAAGCTcTCCGAGCTTGGGTTTGCTGATGCCgg taccggaggtAAGTACTCAGATCTCGAGggaggttccggcGAGCTCAAGCTTCGCGGCGATGGCGAACCGAGCGGCGTGCCGGTGGCGGTGGTGCTGCTGCCGGTGTTTGCGCTGACC CTGGTGGCGGTGTGGGCGTTTGTGCGCTATCGCAAACAGCTGTAGGGATCCACCGGATCTAGATAACTGATCATAATCAGCCATAC
NASP_HDR_upstream_F	AGCTACTCGCCCTGAACATGCAGAGCAGCACTG
NASP_HDR_upstream_R	CGTTCCCCTGAGGTGGCGAACCAGCGAACG
GFPforNASP_HDR_F	TTCGCCACCTCAGGGGAACGATGGTGAGCAAGGGCGAGGA
GFPforNASP_HDR_R	GCTGTGGACTCCATGGCCATATGGCCCTGGAAGTAAAGGT

NASP_HDR_downstream_F	ATGGCCATGGAGTCCACAGCCACTGCCGC
NASP_HDR_downstream_R	TTATATTCCCGGGTTATCCAGGGGTTCTACCAGAGGCACACG
NASP_pair1_upstream_F	CACCGCCATGGCCATCGTTCCCCTG
NASP_pair1_upstream_R	AAACCAGGGGAACGATGGCCATGGC
NASP_pair1_downstream_F	CACCGAGCCACTGCCGCCGTCGCCG
NASP_pair1_downstream_R	AAACCGGCGACGGCGGCAGTGGCTC
ASF1B_UP_R	GGCCATCGCCTCGCCTCGCC
ASF1B_UP_F	AATCACTTCGGGTGCGAGCACC
Spot-tag_mCherry_3C_R	GCACCGACACCTTGGCCATGGGCCCCTGGAACAGAACTTCCAGGAGTCCGGACTTGTACAGCT
Spot-tag_mCherry_3C_F	GAGGCGAGGCGatggccccggatcgcgtgcgcgcggtgagccattggagcagcGTGAGCAAGGGCGAGGAGGA
ASF1B_DOWN_R	GGAAAATGGGAAGGGGCTGGATATTGG
ASF1B_DOWN_F	ATGGCCAAGGTGTCGGTGC
ASF1B_sgRNA_UP_F	CACCGTCGCCTCGCCGCGCCGCAGC
ASF1B_sgRNA_UP_R	AAACGCTGCGGCGCGGCGAGGCGAC
ASF1B_sgRNA_Down_F	CACCGCAAGGTGTCGGTGCTGAACG
ASF1B_sgRNA_Down_R	AAACCGTTCAGCACCGACACCTTGC

Table S3. Antibodies, companies, catalogue number and lot, dilutions used and webpage link

Name	Company	Catalogue number	Lot	Origin	Concentration used	Webpage
Anti-ASF1A (C6E10)	Cell Signaling Technology	C6E10		Rabbit - monoclonal	1:1 k	https://media.cellsignal.com/pdf/2990.pdf
Anti-ASF1B	Cell Signaling Technology	C70E2	2	Rabbit - monoclonal	1:1 k	https://www.cellsignal.co.uk/products/primary-antibodies/asf1b-c70e2-rabbit-mab/2902
Anti-HAT1	Abcam	ab194296	GR239204-4	Rabbit - monoclonal [EPR18775] to KAT1 / HAT1	1:1 k	https://www.abcam.com/kat1--hat1-antibody-epr18775-ab194296.html
Anti-Histone H3	Cell Signaling Technology	#9715	23	Rabbit - polyclonal, IgG	1:1 k	https://www.cellsignal.co.uk/products/primary-antibodies/histone-h3-antibody/9715
Anti-Histone H4	Abcam	ab7311	GR274242-1	Rabbit - polyclonal to Histone H4 - ChIP Grade, IgG	1:1 k	https://www.abcam.com/histone-h4-antibody-chip-grade-ab7311.html
Anti-Histone H4 k12Ac	Millipore (Merck)	#07-595	#3328962	Rabbit - polyclonal	1:1 k	https://www.merckmillipore.com/GB/en/product/Anti-acetyl-Histone-H4-Lys12-Antibody,MM_NF-07-595
Anti-Histone H4 k5Ac	Millipore (Merck)	#07-327	#3307312	Rabbit - polyclonal	1:1 – 5 k	https://www.merckmillipore.com/GB/en/product/Anti-acetyl-Histone-H4-Lys5-Antibody,MM_NF-07-327?ReferrerURL=https%3A%2F%2Fwv
Anti-Importin4	Abcam	ab181037	GR151286-1	Rabbit - monoclonal [EPR13660-27] to Importin4	1:10 k	https://www.abcam.com/importin4-antibody-epr13660-27-ab181037.html
Anti-Karyopherin beta 3 (IPO5)	Abcam	ab88695	GR3031337-1	Mouse polyclonal	1:500 50 µg at 1 mg/ml, secondary at 1: 5 k	https://www.abcam.com/karyopherin-beta-3-antibody-ab88695.html
Anti-mCherry	Abcam	ab167453	GR3265215-1	Rabbit polyclonal	1:5 k	https://www.abcam.com/mcherry-antibody-ab167453.html?productWallTab=ShowAll
Anti-RbAp46/48	Cell Signaling Technology	(D4F8) #9067	1 Ref 10/2017	Rabbit - monoclonal (IgG)	1:1 k	https://www.cellsignal.co.uk/products/primary-antibodies/rbap46-rbap48-d4f8-rabbit-mab/9067?Ntk=Products&Ntt=9067
Anti-UBR7	Abcam	ab241371	GR3262878-3	Rabbit - polyclonal	1:1 k	https://www.abcam.com/ubr7-antibody-ab241371.html
GFP (B-2) HRP	Santa Cruz	sc-9996 HRP	I2618	Mouse - monoclonal (clone B-2), IgG2a	1:1 to 1:15 k	https://datasheets.scbt.com/sc-9996.pdf
Goat Anti-Mouse HRP	Abcam	ab205719	GR247077-9	Goat - polyclonal, IgG	1:5 k	https://www.abcam.com/goat-mouse-igg-hl-hrp-ab205719.html
Anti-Rabbit, HRP-linked antibody	Cell Signaling Technology	7074S	27	Goat - polyclonal, IgG	1:10 – 20 k	https://www.cellsignal.co.uk/products/secondary-antibodies/anti-rabbit-igg-hrp-linked-antibody/7074
Goat Anti-Rabbit Alexa 568	Abcam	ab175471	GR1811195-3	Goat - polyclonal, IgG	1:1 k	https://www.abcam.com/goat-rabbit-igg-hl-alexa-fluor-568-ab175471.html